Micro-displacement tensor

G. Zurlo^{a,*}, L. Truskinovsky^b

^aSchool of Mathematical and Statistical Sciences, University of Galway, University Road,
Galway, Ireland
^bPMMH-ESPCI, 7 Quai Saint-Bernard, 75005 Paris, France

Abstract

We propose an extended kinematics of nominally elastic continuum solids allowing one to describe their mechanical interaction with micro-scale loading devices. The main new ingredient is the concept of a micro-displacement tensor which extends the conventional description of the deforming elastic solids in terms of macroscopic displacement vectors. We show that micro-displacement tensors are particularly useful in dealing with active incompatibility acquisition and its subsequent passive relaxation. We use the proposed approach to describe the energetics of surface deposition while accounting for the presence of micro-mechanical controls. To illustrate the effectiveness of the new conceptual scheme we present two case studies: crystallization from a melt resulting in pre-stress, and winding of a coil with controlled pre-stretch.

Keywords: micro-displacement tensor, incompatibility and residual stress, non-Euclidean solids, bulk and surface growth, 3D printing

1. Introduction

Recent attempts to mimic biological prototypes in technological applications highlight the necessity to extend the conventional kinematic framework of solid mechanics. One of the most important challenges of this type is to learn how to deal in continuum framework with active materials capable of acquiring and manipulating mechanical "information". The latter can be stored in the form of geometric incompatibility [1, 2, 3]. Since such incompatibility can be implanted into a solid material, the question arises how this can be performed in a controlled way. A closely related question is how the stored "information" of this type can be either erased or expanded.

It is well known that the usual defects of crystal lattices representing sources of incompatibility can be generated using conventional macroscopic loads. However, the control of the distribution of such defects is rather limited. An alternative approach, which we pursue in this paper, would be to incorporate incom-

 $Email\ address: \verb"giuseppe.zurlo@universityofgalway.ie" (G.\ Zurlo)$

^{*}Corresponding author

patibility through the interaction of a solid with external micro-scale "agents". The latter can be either integrated into the bulk or act on the surface [4, 5]. A technologically relevant example of a surface related micro-mechanical activity is the interaction of a feeding head of a 3D printer with a deposited elastic material [6, 7] and this will be the main testing ground for the proposed general theory. In this regard the present paper can be viewed as an attempt to generalize the ideas developed in our previous work dedicated to the design of 3D printing algorithms [8, 9, 10].

As already intuitively clear, an uncontrolled surface deposition/insertion of a new material can compromise the compatibility of an emerging elastic solid. It can then become a source of anelasticity manifesting itself through the accumulation of residual stresses [11]. The problem of tempering such stresses comes to the forefront when it is necessary to ensure that the manufactured material responds in specific way to external loads. The corresponding control problem is fundamentally nonlocal, as the final configuration of incompatibility depends on the whole history of the deposition/insertion process.

The processes of surface growth are not only biologically relevant [12, 13], but are also technologically important, as in roll/coil winding and concrete deposition in structures. In fact, they are ubiquitous in nature, as in growth of crystals and gravitational accretion, and therefore the attempts of quantitative mechanical modeling of surface deposition have a long history starting with the pioneering works [14, 15, 16, 17, 18, 19], further elaborated in [20, 21, 22, 23, 24, 25, 26, 27]. More recently, the process of surface deposition/ablation was modeled in the framework of the theory of nonlinear-elastic phase transitions with the non-trivial reference metric serving as a characterization of the reference state of the deposited "phase", e.g. [28, 29, 30, 31, 32, 33, 34, 35, 36, 37]. In such approaches, the advancement of the growth surface was either prescribed, say through the controlled rate of heat removal, or regulated by the kinetics of the "effective" phase transformation.

Here we develop a new model where both the growth rate on the deposition surface and the evolution of the growth-induced incompatibility, emerge as an outcome of the micro-activity of sub-continuum forces. To this end we develop a novel kinematic description of incompatible (Non-Eucleadian) solids allowing one to use continuum mechanical language while dealing with micro-deformations. The main new ingredient of the proposed approach is a non-classical micro-displacement tensor which is absent in the conventional kinematic description of elastic solids focused exclusively on displacement vectors. In the developed framework, generalized forces – representing the mechanical activity of the micro-scale "agents" – emerge naturally as an outcome of a thermodynamically consistent implementation of the extended kinematics of continuum. Since the corresponding micro-displacements are represented by tensors, it is natural that the conjugate micro-forces also emerge as tensorial variables.

To illustrate the developed theory, we present several detailed case studies highlighting different aspects of the proposed quantitative description of micromechanical interactions. Our first example concerns the stability of an interface separating a non-hydrostatically stressed solid from its hydrostatically

loaded melt and viewed in the perspective of surface deposition. While this problem was previously examined in an incompatibility-free setting, our study focuses on the peculiar features of crystallization under controlled pre-stress, which lead to the accumulation of incompatibility and the emergence of residual stresses in the newly formed solid. Our second case study concerns the process of winding of a coil on a solid mandrel with a controlled pre-stretch of the tape. Using this example we illustrate the idea that the acquired inelastic strain depends on the whole time dependent deposition protocol. Our last case study deals with the peculiarities of the viscous relaxation in the bulk of the inelastic strains accumulated during surface deposition. The presented examples allow us to clarify the physical meaning behind the idea of micro-controls and to discuss their actual implementation in realistic situations. We note that the possibility of using the implied micro-scopic "agents" in technological applications opens a new avenue in the design of smart materials and structures, and can be expected to have significant impact on a broad range of engineering disciplines from construction to robotics.

The paper is organized as follows. In Section 2 we use Helmholtz decomposition of elastic distortion to extend the classical kinematic description of macroscopic continuum elastic solids and to introduce the idea of a micro-scale displacement tensor. We then specify the structure of this tensor in the special case of materials with internal layering and present a simplified model of such layering allowing one to bridge microscopic and macroscopic descriptions. In Section 3 the developed extended kinematics is used to address the phenomenon of surface growth. To supplement the purely mechanical description of the underlying activity of the microscopic active "agents" we also present the energetic and thermodynamic closure of the corresponding system of equations allowing one to describe self-consistently the evolution of the growth surface. In Section 4 we illustrate the developed theory by addressing the problem of solidification in a simple geometry. A problem of coil winding, also characterized by simple geometry, is considered in Section 5. In Section 6 we suppress deposition and instead deal with the relaxation of acquired incompatibility. Finally, in Section 7 we summarize our results and discuss potential extensions of the proposed approach.

2. Kinematics of incompatible solids

While remaining in the framework of classical linear elasticity theory we present the symmetric linear elastic strain tensor in the form

$$\boldsymbol{\varepsilon}_e = \operatorname{sym} \nabla \boldsymbol{u} \tag{1}$$

where u = u(x) represents the macroscopic displacement vector at a point x in the stress-free reference configuration; note that in (1) we used the standard notation

$$\operatorname{sym} \mathbf{A} = (\mathbf{A} + \mathbf{A}^{\mathsf{T}})/2$$

for the symmetrization operator applied to an arbitrary second order tensor \mathbf{A} . The simple assumption (1) needs to be modified in the case of non-compatible deformations, where instead of (1) we write

$$\varepsilon_e = \operatorname{sym} \nabla u - \varepsilon_p \tag{2}$$

where the tensorial field $\varepsilon_p(x)$ represents an inelastic (plastic) strain. This implies that this field is not a symmetrized gradient of any displacement field, hence the associated incompatibility tensor is non-trivial:

$$\eta = -\text{CurlCurl}\boldsymbol{\varepsilon}_p \neq \mathbf{0}.$$
(3)

While the field $\varepsilon_p(x)$ formally brings into the theory six functional degrees of freedom, three of them describe the compatible part of inelastic deformation and can be potentially absorbed into the vector field u(x). The remaining three degrees of freedom describe the incompatibility tensor field $\eta(x)$, which is by definition symmetric and divergence free.

2.1. Micro-displacements in the bulk

To characterize the response of incompatible solids whose inelastic strain is generated in the process of surface deposition, we now specialize the expression for the tensor field ε_p by assuming that

$$\varepsilon_e = \operatorname{sym} \left(\nabla \boldsymbol{u} + \operatorname{Curl} \mathbf{U} \right)$$
 (4)

where $\mathbf{U}(x)$ is a new tensor field which we interpret as describing microscopic inelastic displacements. It is clear that, due to its structure, the term containing the tensor field \mathbf{U} cannot be fully reduced to a compatible vector field \mathbf{u} . The implied representation

$$\varepsilon_p = -\text{sym}\left(\text{Curl}\mathbf{U}\right)$$
 (5)

can be interpreted as an attempt to introduce a generalized displacement field responsible for the inelastic strain, which enables a richer kinematics relative to standard compatible elasticity. In what follows, we refer to **U** as the *micro-displacement tensor*.

An irreducible representation of the incompatible tensor fields $\mathbf{U}(x)$, containing only three independent functional degrees of freedom, was proposed by Beltrami [38, 39, 40, 41]. However, for the purpose of describing surface deposition, this representation is overly general, therefore we restrict our attention to a pertinent subclass of micro-displacement tensor fields, still parameterized by three scalar functions.

2.2. Micro-displacements at the boundary

To motivate the adopted structure of the micro-displacement tensor U and to clarify its relation to the process of layered deposition, consider a body \mathcal{B} with boundary $\partial \mathcal{B}$. Introducing the Cauchy stress tensor σ , defined as the derivative

of the elastic energy density $W(\varepsilon_e)$ with respect to the elastic strain, $\sigma = \partial_{\varepsilon_e} W$, we may then use (4) to express

$$\int_{\mathcal{B}} \boldsymbol{\sigma} \cdot \boldsymbol{\varepsilon}_{e} = \int_{\mathcal{B}} \left(-\boldsymbol{u} \cdot \operatorname{Div} \boldsymbol{\sigma} + \mathbf{U} \cdot (\operatorname{Curl} \boldsymbol{\sigma})^{\mathsf{T}} \right) + \int_{\partial \mathcal{B}} \mathcal{T}_{\text{bnd}}$$
(6)

where

$$\mathcal{T}_{\text{bnd}} = \boldsymbol{\sigma} \boldsymbol{n} \cdot \boldsymbol{u} + \boldsymbol{\sigma} \cdot \mathbf{U} (\star \boldsymbol{n})^{\mathsf{T}}. \tag{7}$$

Here the notation $\star n$ is used for the skew-symmetric tensor with axial vector n, defined component-wise by the formula

$$(\star \boldsymbol{n})_{ij} = \varepsilon_{ikj} n_k \tag{8}$$

where ε_{ikj} is the Levi-Civita symbol¹.

The representation of the boundary term (7) suggests that the introduction of the micro-displacement tensor \mathbf{U} enables a richer set of boundary controls compared to standard elasticity. To be more specific, we split the full stress tensor $\boldsymbol{\sigma}$ on the boundary into normal and tangential parts using the definitions

$$s_n := \sigma n, \qquad \sigma_\tau := \mathbf{P}_n \sigma \mathbf{P}_n, \tag{9}$$

where

$$\mathbf{P}_n := \mathbf{I} - \mathbf{n} \otimes \mathbf{n}$$

is the standard surface projection tensor. Note first that s_n is the classical traction vector, which performs work against macroscopic displacements u. To specify the displacements against which the work is performed by the surface (tangential) stress tensor σ_{τ} , we use for the micro-displacement tensor at the boundary $\partial \mathcal{B}$ the ansatz

$$\mathbf{U} = \mathbf{V}_{\tau} \star \mathbf{n} \tag{10}$$

where the tensor \mathbf{V}_{τ} is symmetric and tangential, i.e., $\mathbf{V}_{\tau} = \mathbf{V}_{\tau}^{\mathsf{T}}$ and $\mathbf{V}_{\tau} \mathbf{n} = \mathbf{0}$. Then,

$$\mathcal{T}_{\text{bnd}} = \boldsymbol{s}_n \cdot \boldsymbol{u} + \boldsymbol{\sigma}_{\tau} \cdot \mathbf{V}_{\tau}. \tag{11}$$

Accordingly, the ansatz (10) allows one to set apart the contributions of the normal and tangential components of stress at the boundary.

¹For arbitrary vectors a, b, the tensor $\star a$ acts on b as $(\star a)b = a \times b$, and it satisfies the identity $(\star a)^2 = -\mathbf{P}_a$, where $\mathbf{P}_a = \mathbf{I} - a \otimes a$ is the orthogonal projection onto the plane normal to a. For the sake of notation, we will always intend that the operator \star always acts on the vector at its right side, therefore if for example \mathbf{A} is a tensor and a a vector, by $\mathbf{A} \star a$ we will intend the composition of a tensor \mathbf{A} with the skew-symmetric tensor $\star a$, that is $(\mathbf{A} \star a)_{ij} = A_{i\ell}(\star a)_{\ell j} = A_{i\ell} \varepsilon_{\ell k j} a_k$.

2.3. Layering ansatz

Suppose next that we deal with solid bodies emerging as a result of sequential surface deposition of material layers as in the case of 3D printing. Physically, one can think about solid bodies emerging as a result of sequential surface deposition of material layers, which may be pre-stressed independently. If such body "remembers" the micro-deposition through the associated "frozen" local layering, characterized by the prescribed vector field $\boldsymbol{n}(\boldsymbol{x})$, we may assume that the parametric representation of \mathbf{U} given by (10) holds everywhere in the bulk of the body, so that

$$\mathbf{U}(x) = \mathbf{V}_{\tau}(x) \star n(x) \qquad x \in \mathcal{B}$$
 (12)

where $V_{\tau}(x)$ is a symmetric tensor field which satisfies the constraints

$$\mathbf{V}_{\tau}(\boldsymbol{x})\boldsymbol{n}(\boldsymbol{x}) = \mathbf{0}, \qquad \mathbf{V}_{\tau}(\boldsymbol{x}) = \mathbf{V}_{\tau}(\boldsymbol{x})^{\mathsf{T}}, \qquad \boldsymbol{x} \in \mathcal{B}.$$
 (13)

Because the field V_{τ} is both tangential and symmetric, it can be expressed in a local basis represented by the normal vector field n and two orthogonal vector fields e_1, e_2 that span the plane orthogonal to n:

$$\mathbf{V}_{\tau} = \begin{pmatrix} v_{11} & v_{12} & 0 \\ v_{12} & v_{22} & 0 \\ 0 & 0 & 0 \end{pmatrix} \tag{14}$$

where the three independent parameters are $v_{11}(\mathbf{x})$, $v_{12}(\mathbf{x})$ and $v_{22}(\mathbf{x})$. We can then conclude that the field **U** constrained through (12) carries exactly three independent functional degrees of freedom. Moreover, given that

$$\eta = -\text{CurlCurl}\left(\text{sym}\left(\text{Curl}(\mathbf{V}_{\tau} \star \mathbf{n})\right)\right) \tag{15}$$

the ansatz (12) can be thought as representing an incompatibility tensor η of a generic type since the latter is also symmetric and divergence-free and therefore also carrying exactly three independent functional degrees of freedom.

To further elucidate the physical meaning of the tensor field $\mathbf{V}_{\tau}(\boldsymbol{x})$, we observe that when (12) holds, the average inelastic strain in the body can be written as

$$\overline{\boldsymbol{\varepsilon}}_{p} = \frac{1}{\operatorname{vol}(\mathcal{B})} \int_{\mathcal{B}} \boldsymbol{\varepsilon}_{p} = -\frac{1}{\operatorname{vol}(\mathcal{B})} \int_{\partial \mathcal{B}} \mathbf{V}_{\tau}. \tag{16}$$

We can then write the expression for the average elastic strain in the form

$$\overline{\varepsilon}_e = \frac{1}{\text{vol}(\mathcal{B})} \int_{\partial \mathcal{B}} (\boldsymbol{u} \odot \boldsymbol{n} + \mathbf{V}_{\tau})$$
(17)

where we used the standard definition of the symmetrized tensor product:

$$\boldsymbol{a} \odot \boldsymbol{b} = \operatorname{sym}(\boldsymbol{a} \otimes \boldsymbol{b})$$

for arbitrary vectors a and vector b. To emphasize that V_{τ} in (17) depends on n, we can return to the description of micro-displacements in terms of the

tensor **U** and use its relevant projection $\mathbf{U}_{\tau} := \mathbf{P}_n \mathbf{U} \mathbf{P}_n$ to recast (17) in the form

 $\overline{\varepsilon}_e = \frac{1}{\text{vol}(\mathcal{B})} \int_{\partial \mathcal{B}} \left(\boldsymbol{u} \odot \boldsymbol{n} - \tilde{\mathbf{U}}_{\tau} \otimes \boldsymbol{n} \right), \tag{18}$

where $\tilde{\mathbf{U}}_{\tau} := \mathbf{U}_{\tau} - \frac{1}{2}(\operatorname{tr}\mathbf{U}_{\tau})\mathbf{P}_{n}$ is the deviator of \mathbf{U}_{τ} ; note that in (18) we introduced a new notation

$$\mathbf{A} \otimes \mathbf{a} = \operatorname{sym}(\mathbf{A} \star \mathbf{a})$$

for arbitrary tensor **A** and vector a. The symmetric nature of the relation (18) serves as a reminder that the macro-displacement vector field u(x) and the micro-displacement tensor field $\mathbf{U}(x)$ play parallel and complementary roles in the kinematics of the targeted class of inelastic (incompatible) solids.

2.4. Microscopic perspective

A microscopic interpretation of the tensor field $\mathbf{V}_{\tau}(\mathbf{x})$ is obtained by considering the simplest one-dimensional micro-layering, represented by a stack of thickness ℓ made of m flat elastic layers, each of thickness ℓ/m . As shown in Fig.1, the layers are piled up perpendicularly to a fixed direction n.

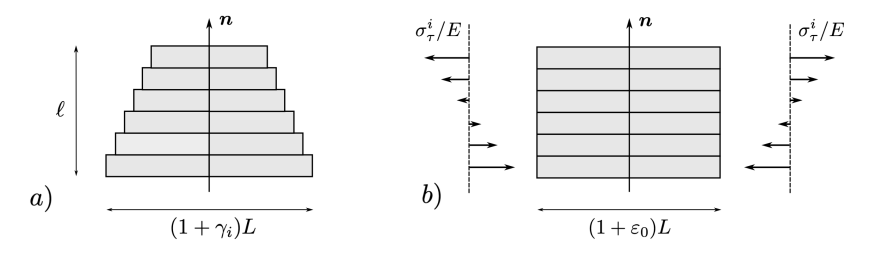


Figure 1: Residual stresses in an incompatible arrangement of m layers, oriented perpendicularly to the direction n. The layers, having initially uneven stress-free lengths, see (a), are stretched or compressed to be of the same size and then glued together, see (b).

Suppose that the layers have different lengths in the reference state, see Fig.1(a) and therefore have to be pre-stressed in order to fit the stack with even length, see Fig.1(b). Denote by $\boldsymbol{\varepsilon}_p^i = \gamma_i \mathbf{P}_n$, with i=1,...,m, the corresponding residual pre-strains which are assumed to be known. To be consolidated into a single stack with uniform length perpendicularly to \boldsymbol{n} , see Fig.1(b), each layer has to be deformed elastically by corresponding lateral tractions σ_{τ}^i , see Fig.1(c). If we assume that the deformation is strictly lateral and we adopt again the framework of classical linear elasticity, we can express the required lateral stress in each layer in the form

$$\sigma_{\tau}^{i} = E(\varepsilon_{0} - \gamma_{i}) \tag{19}$$

where E is an elasticity modulus and ε_0 is the total strain in the assembled stack which, according to our assumption, should be the same for all layers. As the

layers are brought to the same horizontal length, they undergo relative sliding which compensates for the original inhomogeneous uni-axial pre-strain.

Suppose next that the consolidated layers are bonded by a perfect "glue" which prevents subsequent relative sliding. Then the constraints are removed and the resulting composite body is allowed to relax and reach elastic equilibrium. Suppose further that during such relaxation the deformation in each layer is constrained to remain uniaxial, so that no bending can occur.

Due to the presence of the glue, such relaxation must be necessarily homogeneous, with the stack expanding or contracting in the lateral direction. The resulting equilibrated structure will carry residual stresses while not being loaded externally, which means that the composed body will contain embedded distributed incompatibility.

To characterize equilibrium we use the fact that in the relaxed state the resultant force on the lateral edges must be equal to zero, cf. [16]:

$$\sum_{1}^{m} \sigma_{\tau}^{i} = 0. \tag{20}$$

If we substitute (19) into this equation we obtain that

$$\varepsilon_0 \equiv \langle \gamma \rangle := \frac{1}{m} \sum_{1}^{m} \gamma_i \tag{21}$$

where $\langle \gamma \rangle$ is the average inelastic strain in the stack. Therefore, the stress in the stack is

$$\sigma_{\tau}^{i} = E(\langle \gamma \rangle - \gamma_{i}). \tag{22}$$

This expression reveals that the stress in such composite body vanishes if and only if the plastic strains γ_i are uniform. As we now show, this corresponds precisely to the case where the plastic strain becomes compatible and the micro-displacement tensor becomes trivial.

To compute the corresponding micro-displacement tensor, note that the inelastic strain in the stack may be written in the form

$$\varepsilon_p = \sum_{i=1}^m \gamma_i \chi_i(\mathbf{x}) \mathbf{P}_n \tag{23}$$

where $\chi_i(\mathbf{x}) = H(z - z_{i-1}) - H(z - z_i)$ are the characteristic functions which distinguish individual layers, H(z) is the Heaviside function, $z = \mathbf{x} \cdot \mathbf{n}$ is the coordinate perpendicular to the direction of pre-stressing and $z_i = i\ell/m$. If we now rewrite (23) using the decomposition $\varepsilon_p = -\text{sym}(\nabla \mathbf{u} + \text{Curl}\mathbf{U})$, with $\mathbf{U}(\mathbf{x}) = \mathbf{V}_{\tau}(\mathbf{x}) \star \mathbf{n}(\mathbf{x})$, we obtain that the (compatible) macro displacements are of the form

$$\boldsymbol{u}(\boldsymbol{x}) = -\gamma_1 \mathbf{P}_n \boldsymbol{x} \tag{24}$$

whereas the incompatible (micro) displacement tensor is

$$\mathbf{V}_{\tau}(\boldsymbol{x}) = -\mathbf{P}_n \sum_{i=1}^{m-1} [\![\gamma_i]\!] R(z - z_i).$$
(25)

In this expression R(z) = zH(z) is the ramp function, and $[\![\gamma_i]\!] = \gamma_{i+1} - \gamma_i$ are the jumps of strains between neighboring layers.

As noted already from (22), residual stresses vanish when all $[\![\gamma_i]\!] = 0$ throughout the stack, meaning that the jumps $[\![\gamma_i]\!]$ are a direct measure of incompatibility under the assumed kinematic constraints, and they also explicitly appear in the micro-displacement tensor describing the incompatible displacements.

2.5. Micro-displacement tensor and second order structured deformations

Given that in the discrete model discussed in the previous subsection, the micro-displacement tensor $\mathbf{U}(x)$ emerges due to discontinuous strains in the neighboring layers, it is natural to link it to the nonclassical macro-variables introduced in the theory of second-order structured deformations [42].

We begin with the observation that strain discontinuities serve in general as sources for micro-displacement tensors **U**. Consider for instance a finite body textured by a sequence of infinitesimally thin internal layers \mathcal{L}_i of thickness $h = \ell/m$, where ℓ is the fixed characteristic length of the body. Assume that each layer undergoes a compatible distortion $\nabla \tilde{u}_i$, which may be discontinuous across the jump surface $\mathcal{J}(\nabla \tilde{u}_i)$ separating \mathcal{L}_i and \mathcal{L}_{i+1} , cf. [43]. In the corresponding continuum description we can introduce the plastic strain

$$\boldsymbol{\varepsilon}_p = -\operatorname{sym}(\boldsymbol{\beta}_p). \tag{26}$$

Here the inelastic distortion

$$\boldsymbol{\beta}_p = -(\operatorname{Curl} \mathbf{U})^{\mathsf{T}} \tag{27}$$

should be understood as the limit

$$\beta_p = \lim_{m \to \infty} \sum_{i=1}^{m} (\nabla \tilde{\boldsymbol{u}}_i) \, \chi(\mathcal{L}_i)$$
 (28)

where $\chi(\mathcal{L}_i)$ is the characteristic function of layer \mathcal{L}_i . The corresponding Nye tensor [44] takes the form

$$\mathbf{G} = \operatorname{Curl}\boldsymbol{\beta}_{p} = \lim_{m \to \infty} \sum_{i=1}^{m} (\star \boldsymbol{n}_{i}) \llbracket \nabla \tilde{\boldsymbol{u}}_{i} \rrbracket^{\mathsf{T}} \delta_{i}$$
 (29)

where δ_i is the two-dimensional Dirac measure supported on the jump surface $\mathcal{J}(\nabla \tilde{u}_i)$, and n_i is its unit normal.

The representation (27) suggests that

$$\Delta \mathbf{U} = \mathbf{G}^{\mathsf{T}} \tag{30}$$

and therefore [45]

$$\mathbf{U}(\boldsymbol{x}) = -\frac{1}{4\pi} \int_{\mathbb{R}^3} \frac{1}{\rho(\boldsymbol{x}, \boldsymbol{y})} \mathbf{G}^{\mathsf{T}}(\boldsymbol{y}) \, dV(\boldsymbol{y})$$
(31)

where we considered for simplicity an unbounded domain and used the notations $\varrho(\boldsymbol{x},\boldsymbol{y}) = \|\boldsymbol{x} - \boldsymbol{y}\|$ for the Euclidean distance between points \boldsymbol{x} and \boldsymbol{y} and $dV(\boldsymbol{y})$ for the volume element centered at \boldsymbol{y} . Substituting (29) into (31), we conclude that away from the boundaries of the body

$$\mathbf{U}(\boldsymbol{x}) = \lim_{m \to \infty} \sum_{i=1}^{m} \frac{1}{4\pi} \int_{\mathcal{B} \cap \mathcal{J}(\nabla \tilde{\boldsymbol{u}}_i)} \frac{1}{\varrho(\boldsymbol{x}, \boldsymbol{y})} [\![\nabla \tilde{\boldsymbol{u}}_i(\boldsymbol{y})]\!] \star \boldsymbol{n}_i(\boldsymbol{y}) \, dA_i(\boldsymbol{y}). \tag{32}$$

Formulas similar to (32), but involving an additional "localization", are employed in the theory of second-order structured deformations to define macroscopic observables that account for microscale "corrections" to the conventional second gradients of the macroscopic fields u(x), see, e.g., [42]. However, these corrections remain local. In contrast, in our theory, the corresponding macroscopic observables aim to "correct" the macroscopic displacement field u(x) in a strongly nonlocal manner. Nevertheless, in both approaches, the jump discontinuities of the deformation gradient play a central role, giving rise to novel kinematical descriptors that emerge through the associated averaging, with or without concurrent localization.

3. Surface deposition

To illustrate the effectiveness of the proposed kinematic extension of the conventional elastic continuum model, we now turn to surface deposition. In particular, since this phenomenon involves continuous addition of prestressed layers of matter to the external boundary of a body, it is a natural playground for checking the validity of our ansatz for the micro-displacement tensor.

Observe first that the process of surface deposition implies the existence of an evolving reference domain \mathcal{B}_t , where t is time. Suppose that the new layers of material are continuously deposited on the external boundary of this domain $\Omega_t = \partial \mathcal{B}_t$. The latter may be defined by the corresponding surface coordinates $\boldsymbol{\xi} = (\xi_1, \xi_2)$ and by the mapping

$$x = \psi(\xi, t). \tag{33}$$

The function $\psi(\boldsymbol{\xi},t)$ can be always chosen in such a way that the vector $\dot{\psi}(\boldsymbol{\xi},t)$ is normal to Ω_t , where the dot denotes differentiation with respect to time. Thus we can then write

$$\dot{\boldsymbol{\psi}} = D\boldsymbol{n} \tag{34}$$

where n is the normal to the surface Ω_t and $D = ||\dot{\psi}||$ is the normal velocity of Ω_t . Equivalently, the growth surface may be represented as the level-set of a function

$$\vartheta(\mathbf{x}) = t \tag{35}$$

such that $\vartheta(\psi(\boldsymbol{\xi},t)) = t$ for all $\boldsymbol{\xi}$. We can then write

$$\boldsymbol{n}(\boldsymbol{x}) = D\nabla\vartheta\tag{36}$$

and therefore

$$D(\mathbf{x}) = ||\nabla \theta||^{-1}. \tag{37}$$

Note that according to (36) the local orientation of the layers past their acquisition remains fixed, which means that the vector field n = n(x) is effectively "frozen".

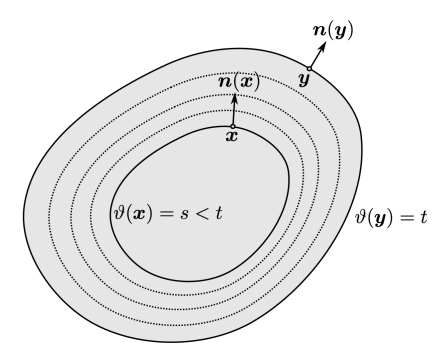


Figure 2: The growing body which retains a memory of its internal layering emerging during the deposition process. The local orientation of the layer n(x) is determined at the moment when the growth surface passes through the point x and remains unchanged thereafter.

3.1. Dynamics

To formulate thermodynamically consistent dynamic theory of surface growth, we can use the conventional machinery of continuum mechanics. We assume that the material model is fully characterized by the specific free energy density $W(\varepsilon_e)$ which is a function of the linear elastic strain tensor $\varepsilon_e(\boldsymbol{x},t)$ defined for $\boldsymbol{x} \in \mathcal{B}_t$ by the relation

$$\varepsilon_e = \operatorname{sym} \left(\nabla \boldsymbol{u} + \operatorname{Curl}(\mathbf{V}_\tau \star \boldsymbol{n}(\boldsymbol{x})) \right) \tag{38}$$

where u(x,t) is the evolving macro-displacement vector field and $\mathbf{V}_{\tau}(x,t)$ is the evolving micro-displacement tensor tangential field, satisfying

$$\begin{cases}
\mathbf{V}_{\tau}(\boldsymbol{x},t) = \mathbf{V}_{\tau}^{\mathsf{T}}(\boldsymbol{x},t) \\
\mathbf{V}_{\tau}(\boldsymbol{x},t)\boldsymbol{n}(\boldsymbol{x}) = \mathbf{0}.
\end{cases}$$
(39)

The next step is to compute the rate of change of the elastic energy $\mathcal{E} = \int_{\mathcal{B}_t} W$ while taking into account the time dependence of \mathcal{B}_t . Using standard transformations we obtain

$$\dot{\mathcal{E}} = \int_{\mathcal{B}_{t}} \left(-\dot{\boldsymbol{u}} \cdot \operatorname{Div}\boldsymbol{\sigma} - \dot{\mathbf{V}}_{\tau} \cdot \operatorname{Curl}_{n}\boldsymbol{\sigma} \right) +$$

$$\int_{\Omega_{t}} \left(\mathring{\boldsymbol{u}} \cdot \boldsymbol{\sigma} \boldsymbol{n} + \mathring{\mathbf{V}}_{\tau} \cdot \boldsymbol{\sigma}_{\tau} \right) +$$

$$\int_{\Omega_{t}} D\left(W - \boldsymbol{\sigma} \boldsymbol{n} \cdot \partial_{n} \boldsymbol{u} - \boldsymbol{\sigma}_{\tau} \cdot \partial_{n} \mathbf{V}_{\tau} \right),$$

$$(40)$$

where $\sigma = \partial_{\varepsilon_e} W$ is the Cauchy stress while $\sigma_{\tau} := \mathbf{P}_n \sigma \mathbf{P}_n$ is the surface stress at the boundary. We denoted by ∂_n the directional derivative along \boldsymbol{n} , and used convective derivatives as in $\boldsymbol{\dot{u}} := \dot{\boldsymbol{u}} + D \, \partial_n \boldsymbol{u}$ and $\mathring{\mathbf{V}}_{\tau} := \dot{\mathbf{V}}_{\tau} + D \, \partial_n \mathbf{V}_{\tau}$. In addition, we introduced a new notation

$$\operatorname{Curl}_{n} \boldsymbol{\sigma} = -\mathbf{P}_{n} \operatorname{sym} \left((\star \boldsymbol{n}) \operatorname{Curl} \boldsymbol{\sigma} \right) \mathbf{P}_{n}. \tag{41}$$

Assume next that the external power can be written in the form:

$$\mathcal{P} = \int_{\Omega_t} \left(\mathbf{s}_n \cdot \mathbf{\dot{u}} + \boldsymbol{\sigma}_a \cdot \mathbf{\dot{V}}_{\tau} + W_a D \right) + \int_{\mathcal{B}_t} \left(\mathbf{b} \cdot \mathbf{\dot{u}} + \mathbf{B}_a \cdot \mathbf{\dot{V}}_{\tau} \right). \tag{42}$$

Here s_n is the classical surface traction while b introduces classical bulk force. The last term in the surface integral in (42) (proportional to D) is also classical, with the constant W_a representing the reference energy of the deposited material.

The remaining terms in (42), proportional to $\dot{\mathbf{V}}_{\tau}$ in the bulk and $\dot{\mathbf{V}}_{\tau}$ on the surface Ω_t , are new. They can be viewed as representing the microscopic "activity" involved in the creation of incompatibility. Specifically, the incompatibility buildup on the deposition surface Ω_t , is driven by the tensorial "generalized forces" $\boldsymbol{\sigma}_a$. Similarly, the incompatibility creation in the bulk of \mathcal{B}_t is controlled by the tensorial "generalized forces" \mathbf{B}_a . In view of the special structure of the tensor \mathbf{V}_{τ} , the conjugate tensorial fields \mathbf{B}_a and $\boldsymbol{\sigma}_a$ are symmetric and tangential so that that $\mathbf{B}_a = \mathbf{B}_a^{\mathsf{T}}$, $\mathbf{B}_a \boldsymbol{n} = \mathbf{0}$ and $\boldsymbol{\sigma}_a = \boldsymbol{\sigma}_a^{\mathsf{T}}$, $\boldsymbol{\sigma}_a \boldsymbol{n} = \mathbf{0}$.

We are now in a position to derive the dynamic equations of the model including the equation governing the evolution of the micro-displacement tensor. For simplicity we ignore inertial effects and neglect the conventional viscosity. We also assume that the system is isothermal. Then we can compute the dissipation rate

$$\mathcal{P} - \dot{\mathcal{E}} = \mathcal{D} = \int_{\mathcal{B}_{t}} \dot{\boldsymbol{u}} \cdot (\boldsymbol{b} + \operatorname{Div}\boldsymbol{\sigma}) + \int_{\mathcal{B}_{t}} \dot{\mathbf{V}}_{\tau} \cdot (\mathbf{B}_{a} + \operatorname{Curl}_{n}\boldsymbol{\sigma}) + \int_{\Omega_{t}} \dot{\boldsymbol{u}} \cdot (\boldsymbol{s}_{n} - \boldsymbol{\sigma}\boldsymbol{n}) + \int_{\Omega_{t}} \dot{\mathbf{V}}_{\tau} \cdot (\boldsymbol{\sigma}_{a} - \boldsymbol{\sigma}_{\tau}) + \int_{\Omega_{t}} D(W_{a} - W + \boldsymbol{\sigma}\boldsymbol{n} \cdot \partial_{n}\boldsymbol{u} + \boldsymbol{\sigma}_{\tau} \cdot \partial_{n}\mathbf{V}_{\tau}) \geq 0.$$

$$(43)$$

We assume for simplicity that the mechanical response, associated with the macroscopic rates $\dot{\boldsymbol{u}}$ in the bulk of the domain \mathcal{B}_t and $\dot{\boldsymbol{u}}$ on the growth surface Ω_t , is purely elastic and therefore dissipation free. We can then localize the corresponding terms in (43) to obtain the field equations

$$\mathcal{B}_t: \quad \text{Div } \boldsymbol{\sigma} + \boldsymbol{b} = \boldsymbol{0} \tag{44}$$

and the boundary conditions

$$\Omega_t: \quad \boldsymbol{\sigma} \boldsymbol{n} = \boldsymbol{s}_n. \tag{45}$$

For the microscopic displacements we assume the simplest overdamped relaxational dynamics. Specifically we assume that the dissipative potential is an isotropic quadratic function of the non-classical rates $\dot{\mathbf{V}}_{\tau}$ in the bulk of the domain \mathcal{B}_t and $\mathring{\mathbf{V}}_{\tau}$ on the growth surface Ω_t . This gives the kinetic equations in the bulk

$$\mathcal{B}_t: \quad \mathbf{B}_a + \mathbf{Curl}_n \boldsymbol{\sigma} = \alpha \dot{\mathbf{V}}_\tau \tag{46}$$

that is supplemented by the corresponding boundary conditions

$$\Omega_t: \quad \boldsymbol{\sigma}_a - \boldsymbol{\sigma}_\tau = \gamma \mathring{\mathbf{V}}_\tau. \tag{47}$$

Note that in (46) and (47) we introduced the phenomenological coefficients $\alpha \geq 0$ and $\gamma \geq 0$ characterizing the associated volumetric and surface relaxation rates, respectively. Finally, if we similarly assume that the deposition rate $\dot{\psi}$ is not prescribed and, instead, we associate with it a quadratic dissipative potential, we obtain kinetic relation regulating the surface growth process in the form

$$\Omega_t: W_a - W + \sigma n \cdot \partial_n u + \sigma_\tau \cdot \partial_n V_\tau = \beta D \tag{48}$$

where $\beta \geq 0$ is another phenomenological coefficient.

3.2. Limiting regimes

We now discuss some physically relevant special regimes emerging as we make particular assumptions regarding the relative values of the (appropriately nondimensionalized) phenomenological rate constants α , β and γ .

For instance, in the limiting case $\gamma = 0$, meaning physically that the associated relaxation time is small at the time scale of the evolution of the system, we essentially assume that the equilibration on the boundary is infinitely fast. Then our Eq. (47) reduces to an equality

$$\Omega_t: \quad \boldsymbol{\sigma}_{\tau} = \boldsymbol{\sigma}_a. \tag{49}$$

Under this assumption, the tangential component of the stress tensor σ on the growth surface is tightly controlled by the externally imposed "generalized forces" σ_a . Together with (45), this implies that the entire stress tensor is prescribed on the deposition surface. This constitutive choice was adopted, for instance, in our previous works [8, 9, 10]. In the absence of experimental evidence suggesting otherwise, we also adopt (49) as one of the boundary conditions in the present study.

The opposite limit, $\gamma = \infty$, effectively suggests that

$$\Omega_t: \quad \mathring{\mathbf{V}}_{\tau} = \mathbf{0}. \tag{50}$$

In this case the micro-displacement tensor would have to be externally controlled on the boundary. Note that for finite values of γ , the evolution described by (49) may account, for example, for slippage between the newly added layers and the existing body, see for instance a related discussion in [36].

Another important limiting case is when $\beta = 0$ in (48), meaning that the growth surface is always in equilibrium as the attachment kinetics is formally instantaneous. This would mean that instead of (48) we should use

$$\Omega_t: \quad W_a - W + \mathbf{s}_n \cdot \partial_n \mathbf{u} + \boldsymbol{\sigma}_a \cdot \partial_n \mathbf{V}_{\tau} = 0 \tag{51}$$

wherein wa used (49). Note that in addition to the conventional macroscopic elasto-static Eshelby force $W - \mathbf{s}_n \cdot \partial_n \mathbf{u}$ we have in (51) a matching microscopic (active) contribution $W_a + \boldsymbol{\sigma}_a \cdot \partial_n \mathbf{V}_{\tau}$.

In the opposite limiting regime $\beta = \infty$, when growth is fully suppressed, the boundary condition (48) is replaced by the condition

$$\Omega_t: \quad D = 0 \tag{52}$$

meaning that no boundary deposition is taking place.

Yet another interesting limiting case is when $\alpha = 0$ in (46) and the bulk relaxation of the field \mathbf{V}_{τ} is instantaneous. In this case we obtain the bulk equilibrium equation

$$\mathcal{B}_t: \quad \operatorname{Curl}_n \boldsymbol{\sigma} + \mathbf{B}_a = \mathbf{0} \tag{53}$$

suggesting that the "generalized force" \mathbf{B}_a fully governs $\mathrm{Curl}_n \boldsymbol{\sigma}$, consistent with our other implicit assumption that the physical macroscopic force \boldsymbol{b} controls $\mathrm{Div}\boldsymbol{\sigma}$. In this context, the externally imposed tensor field \mathbf{B}_a acts as a source of incompatibility, giving rise to the associated residual stresses. In the context of our microscopic model, the field \mathbf{B}_a can be interpreted as representing the externally applied system of micro-forces acting within the stack of parallel layers. It effectively serves as a "glue" that prevents relative sliding between layers, thereby preserving the jumps in reference strains across neighboring layers.

In the opposite limiting regime $\alpha = \infty$ we obtain from (46) that

$$\mathcal{B}_t: \quad \dot{\mathbf{V}}_\tau(\boldsymbol{x}, t) = \mathbf{0} \tag{54}$$

and therefore $\mathbf{V}_{\tau} = \mathbf{V}_{\tau}(\boldsymbol{x}) = \mathbf{V}_{\tau}(\boldsymbol{x}, \vartheta(\boldsymbol{x}))$. This means that the micro-displacement tensor does not evolve past the moment of deposition and therefore the incompatibility acquired at deposition is effectively "frozen".

3.3. Relaxation of incompatibility

As already indicated, the micro-displacement tensor field $\mathbf{V}_{\tau}(\boldsymbol{x},t)$ can contain, in principle, not only an incompatible part which is responsible for the emergence of a non-trivial incompatibility tensor field $\eta(\boldsymbol{x},t)$, but also a compatible part which can be, in principle, absorbed into the macro-displacement vector field $\boldsymbol{u}(\boldsymbol{x},t)$. As we see from the examples considered later in the paper, this is indeed the case even under very restricted geometric assumptions. The apparent contradiction with our assumption that the fields $\mathbf{V}_{\tau}(\boldsymbol{x},t)$ and $\boldsymbol{u}(\boldsymbol{x},t)$ are independent, would not pose any problem if the adopted relaxation model for the field $\mathbf{V}_{\tau}(\boldsymbol{x},t)$ would concern only its incompatible component. While the general analysis of this problem is beyond the task of this paper, we can still provide some arguments in support of the conjecture that the dynamics of the incompatible part of $\mathbf{V}_{\tau}(\boldsymbol{x},t)$ is largely independent from the evolution of its compatible part.

For simplicity, we consider the special case when the external sources potentially driving the production of incompatibility are absent. Specifically, assume

that the (passive) bulk vectorial forces and the (active) bulk tensorial forces can be neglected, so that

$$\mathcal{B}_t: \quad \boldsymbol{b} = \boldsymbol{0}, \qquad \mathbf{B}_a = 0 \tag{55}$$

In this case, the dynamic equations reduce to

$$\mathcal{B}_t$$
: Div $\boldsymbol{\sigma} = \mathbf{0}$, Curl $_n \boldsymbol{\sigma} = \alpha \dot{\mathbf{V}}_{\tau}$ (56)

where the rate of relaxation of $\mathbf{V}_{\tau}(\boldsymbol{x},t)$, governed by (56)₂, is controlled by the parameter α . The question is whether such relaxation impacts both compatible and incompatible components of $\mathbf{V}_{\tau}(\boldsymbol{x},t)$ or it actually concerns only the incompatible part of $\mathbf{V}_{\tau}(\boldsymbol{x},t)$, while leaving the corresponding compatible component intact.

To at least partially answer this question it is necessary to obtain a description of the final post-relaxation state described by the equations

$$\mathcal{B}_t$$
: Div $\boldsymbol{\sigma} = \mathbf{0}$, Curl $_n \boldsymbol{\sigma} = \mathbf{0}$. (57)

Even this limited question cannot be addressed here in full generality, and instead we consider the simpler problem of characterizing solutions of the system

$$\begin{cases} \operatorname{Div} \boldsymbol{\sigma} = \mathbf{0}, \\ \operatorname{sym}(\operatorname{Curl} \boldsymbol{\sigma}) = \mathbf{0}. \end{cases}$$
 (58)

One can see that we replaced the special operator $\operatorname{Curl}_n\sigma$ relying on the existence of a "frozen" field n(x) by a more general one, $\operatorname{sym}(\operatorname{Curl}\sigma)$. To justify this choice we note that in all examples considered later in the paper, the special choice of the deposition geometry (radial and planar) ensures that such special and general problems are fully equivalent.

Observe first that for isotropic linear elastic materials, one can construct a class of nontrivial *compatible* deformations with $\varepsilon_e = \text{sym} \nabla u$ which solves equations (58). Indeed, in this case, the system (58) takes the form

$$\begin{cases} \mu \Delta \boldsymbol{u} + (\mu + \lambda) \nabla \text{Div} \boldsymbol{u} = \boldsymbol{0}, \\ \text{sym}(\nabla \text{Curl} \boldsymbol{u}) = \boldsymbol{0} \end{cases}$$
 (59)

where we introduced Lamé constants μ and λ . Note next that $(59)_1$ can be also rewritten as

$$\nabla \text{Div} \boldsymbol{u} = \frac{\mu}{2\mu + \lambda} \text{CurlCurl} \boldsymbol{u}. \tag{60}$$

From $(59)_2$ we now infer that the gradient of Curl u is a skew-symmetric tensor field that can be represented in the form [46]

$$Curl u = a + c \times x \tag{61}$$

where a and c are constant vectors. After substituting (61) into (60) and upon integration we obtain

$$Div \boldsymbol{u} = \frac{2\mu}{2\mu + \lambda} \boldsymbol{c} \cdot \boldsymbol{x} + C \tag{62}$$

where C is a constant. Therefore, by using the obtained information we can characterize the field u(x) through its Helmholtz decomposition

$$\boldsymbol{u} = \nabla \varphi + \operatorname{Curl} \boldsymbol{\omega} \tag{63}$$

where the scalar field φ and the solenoidal vector field ω can be found from the equations

$$\begin{cases}
\Delta \varphi = \frac{2\mu}{2\mu + \lambda} \mathbf{c} \cdot \mathbf{x} + C \\
\Delta \omega = -\mathbf{a} - \mathbf{c} \times \mathbf{x}.
\end{cases} (64)$$

We can therefore conclude that, by finding constants $(\boldsymbol{a}, \boldsymbol{c}, C)$ that are compatible with the boundary conditions, one can specify the compatible component of $\mathbf{V}_{\tau}(\boldsymbol{x},t)$ that is not affected by the relaxation mechanism implied in (58).

Although it cannot be excluded that this mechanism might leave some other compatible component of $\mathbf{V}_{\tau}(\boldsymbol{x},t)$ unrelaxed, the examples discussed in this work show that this does not occur. The only component of $\mathbf{V}_{\tau}(\boldsymbol{x},t)$ involved in the relaxation process is the one carrying incompatibility. Conversely, the compatible component, which remains unaffected by relaxation, is of the form $\operatorname{sym}(\operatorname{Curl}\mathbf{U}) = \operatorname{sym}\nabla\hat{\boldsymbol{u}}$, with $\hat{\boldsymbol{u}}$ exactly given by (64).

3.4. Reduced description

Here we demonstrate how the surface deposition problem can be explicitly solved without any reference to the micro-displacement tensor $\mathbf{V}_{\tau}(\boldsymbol{x},t)$ in the physically relevant special case when $\gamma=0$ and $\alpha=\infty$ simultaneously. Such reduced description is possible due to the complete decoupling of micro and macro problems which are, of course, tightly coupled in the general case.

To focus on the decoupling issue we simplify the problem even further by assuming that the evolution of the deposition surface is not determined self-consistently, but is instead prescribed independently. In other words, we assume that the function $\vartheta(x)$ is given. In this limited setting, the six components of the inelastic strain $\varepsilon_p(x)$ are fully determined at the moment of deposition through six boundary conditions. Suppose that three of them impose the "generalized forces" σ_a

$$\Omega_t: \qquad \boldsymbol{\sigma}_{\tau}(\boldsymbol{x}, \vartheta(\boldsymbol{x})) = \boldsymbol{\sigma}_a(\boldsymbol{x})$$
 (65)

while the other three

$$\Omega_t: \quad \boldsymbol{u}(\boldsymbol{x}, \vartheta(\boldsymbol{x})) = \mathbf{0}$$
 (66)

imply that the displacements attributed to material points become meaningful only after the instant of their deposition. Note that since in this oversimplified setting the inelastic strain $\varepsilon_p(x)$ remains "frozen" after the instant of deposition, we also have $\mathbf{V}_{\tau} = \mathbf{V}_{\tau}(x)$ which represents the decoupling of the the microproblem. The remaining macro-problem reduces to finding the evolution of the displacement field u(x,t).

Note next that the field $\varepsilon_p(x)$ can be eliminated by switching to an incremental formulation. Specifically, given that

$$\sigma(\mathbf{x},t) = \mathbb{C}\varepsilon_e(\mathbf{x},t) \tag{67}$$

and

$$\varepsilon_e(\mathbf{x}, t) = \operatorname{sym} \nabla \mathbf{u}(\mathbf{x}, t) - \varepsilon_p(\mathbf{x})$$
(68)

we can write an incremental constitutive relation in the form

$$\dot{\boldsymbol{\sigma}}(\boldsymbol{x},t) = \mathbb{C}(\operatorname{sym}\nabla\dot{\boldsymbol{u}}(\boldsymbol{x},t)). \tag{69}$$

The associated incremental equilibrium equation is

$$\mathcal{B}_t$$
: Div $\dot{\boldsymbol{\sigma}}(\boldsymbol{x},t) = \mathbf{0}$. (70)

To obtain the incremental boundary condition we differentiate the identity

$$\sigma(x, \vartheta(x)) = \overline{\sigma}(x) \tag{71}$$

with

$$\overline{\sigma}(x) = \sigma_a(x) + s_n \otimes n + n \otimes s_n - (s_n \cdot n)n \otimes n$$
(72)

to obtain

$$\Omega_t$$
: $\dot{\boldsymbol{\sigma}}(\boldsymbol{x}, \vartheta(\boldsymbol{x})) \boldsymbol{n}(\boldsymbol{x}) = D(\boldsymbol{x}) \text{Div} \overline{\boldsymbol{\sigma}}(\boldsymbol{x})$ (73)

where D is the prescribed normal velocity of the deposition surface.

One can see that the ensuing problem for the incremental displacement $\dot{\boldsymbol{u}}(\boldsymbol{x},t)$ is purely elastic. After solving a sequence of such incremental problems, one can reconstruct the time dependent stress and displacement fields at time t using the relations:

$$\begin{cases}
\boldsymbol{\sigma}(\boldsymbol{x},t) = \overline{\boldsymbol{\sigma}}(\boldsymbol{x}) + \int_{\vartheta(\boldsymbol{x})}^{t} \dot{\boldsymbol{\sigma}}(\boldsymbol{x},\tau) d\tau \\
\boldsymbol{u}(\boldsymbol{x},t) = \int_{\vartheta(\boldsymbol{x})}^{t} \dot{\boldsymbol{u}}(\boldsymbol{x},\tau) d\tau.
\end{cases} (74)$$

This completes the solution of the macro-problem, which is then indeed fully decoupled from the problem of identifying the associated micro-displacement tensor.

To address the latter, we can use the obtained function u(x,t) and the six closure conditions (65) and (66) to recover the distribution of the "frozen" inelastic strain

$$\varepsilon_{v}(\boldsymbol{x}) = \mathbb{C}^{-1} \overline{\boldsymbol{\sigma}}(\boldsymbol{x}) - \operatorname{sym}(\nabla \boldsymbol{u}(\boldsymbol{x}, \vartheta(\boldsymbol{x}))).$$
 (75)

Note that in view of (74) the obtained function $\varepsilon_p(x)$ depends non-locally on the controls $s_n(x)$ and $\sigma_a(x)$. To show this more explicitly, we differentiate (65)₂ to obtain

$$\nabla u(x, \vartheta(x)) = -\dot{u}(x, \vartheta(x)) \otimes \nabla \vartheta(x). \tag{76}$$

Equation (76) suggests that the inelastic strain at a point \boldsymbol{x} depends not only on the controls applied in this point at the instant of deposition, but also on the value of the incremental macro-displacement, which in turn depends on the entire prior deposition history. Accordingly, the acquired incompatibility $\boldsymbol{\eta} = \operatorname{CurlCurl}\boldsymbol{\varepsilon}_p$ also inherits the non-local dependence on the applied controls.

For instance, to ensure that $\eta=0$ and therefore the grown body is free of residual stresses, the protocol of applying the "active" stress $\overline{\sigma}$ must be specifically engineered.

After the decoupled incremental macro-problem is solved, the associated micro-displacements described by the "frozen" tensor field $\mathbf{V}_{\tau}(\boldsymbol{x})$ can be reconstructed by inverting the differential relation

$$\varepsilon_p(\mathbf{x}) = -\operatorname{sym}(\operatorname{Curl}(\mathbf{V}_{\tau}(\mathbf{x}) \star \mathbf{n}(\mathbf{x}))) \tag{77}$$

where the field n(x) is assumed to be known. While we are not going to address this problem here in its full generality, our examples show how this can be done in special geometries.

3.5. Coupled problem

We have seen that, in a special limiting case, the incremental macro-problem can be decoupled from the "frozen" micro-problem and solved in a fairly general setting. Such analytical transparency, however, is the exception rather than the rule. The fully coupled problem, incorporating for instance a self-consistent description of surface evolution, or addressing the mechanism of relaxation of the accumulated incompatibility, can be expected to pose significant analytical challenges.

In particular the decoupling of the macroscopic description would not be usually possible, because the growth process is ultimately of micro-scale origin, involving active mechanical interactions which do not reduce to the action of surface-associated active "agents", but also involve bulk evolution driven by the corresponding distributed volumetric "active" agents. The presence of micro-scale mechanical controls/constraints leads to the emergence of inelastic deformations and incompatibility encoded in the evolution of the micro-displacement tensor, which is no longer fully described by the deposition protocol itself.

In the next sections we present a detailed study of several special problems where, due to the assumed radically simplified geometry, one can explore the effect of different active protocols and illustrate various conceptually challenging features of the proposed general theory.

4. Activity assisted solidification

As a first illustration of our approach, consider a process of crystallization from a liquid state interpreted as a growth of a non-hydrostatically stressed elastic crystal from its melt. While this problem in its classical setting is generally regarded as well understood, see for instance, [47, 48, 49, 50, 51, 52, 53, 54, 55, 56, 57, 58, 59, 60, 61], our focus will be on the relatively new question regarding the potential role played by active "agents" on the development of incompatibility during crystallization. For analytical transparency, our analysis will be restricted to isotropic solids and will be carried under the assumptions of physically and geometrically linear elasticity. To emphasize the role of micromechanical actions in the development of incompatibility, we also drastically

simplify the thermal part of the problem by considering crystallization as an isothermal process, while neglecting in this way important aspects of solidification process related to thermo-mechanical coupling [35].

4.1. Problem setting

Consider a solid body of cylindrical shape whose height $\psi(t)$ is a function of time due to the process of surface crystallization from a melt, see Fig. 3. Suppose that the material coordinates in the reference configuration of a solid body are

$$x = re_r + zk \tag{78}$$

where $z \in (0, \psi(t))$ is the axial coordinate, $r \in (0, R)$ is the radial coordinate and e_r is the unit vector in the radial direction. Assume further that the layering of deposited material is horizontal with $n(x) \equiv k$ and that the position of the deposition surface at time t is $z = \psi(t)$.

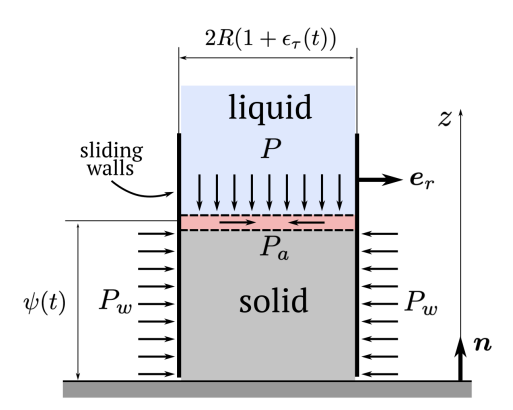


Figure 3: Schematic representation of a solid under non-hydrostatic stress, in contact with its melt. Vertical sliding walls enforce homogeneous lateral deformation, with tractions $s_w = -P_w e_r$. The liquid experiences a hydrostatic pressure $s_n = -Pn$ with (P > 0). The growth front, positioned at $\psi(t)$, carries controllable "active" surface stress $\sigma_a = -P_a$.

We employ a semi-inverse approach and we introduce several assumptions constraining the nature of the emerging deformation. Specifically, we assume that the macro-displacement vector field is of the form

$$\boldsymbol{u}(\boldsymbol{x},t) = u(z,t)\boldsymbol{k} + r\,\epsilon_{\tau}(t)\boldsymbol{e}_{r}(\boldsymbol{x}). \tag{79}$$

Under this assumption, the macroscopic deformation of the growing cylindrical solid body can be represented as an elongation/shortening in the axial direction described by the z-dependent function u(z,t), together with a superimposed uniform shrinking - expansion in the tangential direction described by a z-independent strain variable $\epsilon_{\tau}(t)$. In this way we also assume implicitly that at z=0, only the vertical displacements are constrained by the rigid foundation.

Our assumptions regarding the structure of the micro-displacements can be formulated in the form of an ansatz

$$\mathbf{V}_{\tau}(\boldsymbol{x},t) = v(z,t)\mathbf{P}_{\boldsymbol{k}} \tag{80}$$

where $\mathbf{P}_{k} = \mathbf{I} - \mathbf{k} \otimes \mathbf{k}$ and where the sub-continuum nature of the function v(z,t) should be understood in the sense of (25). In terms of (14), we are effectively assuming that $v_{11} = v_{22} = v(z,t)$ and $v_{12} = 0$. The corresponding inelastic strain is then

$$\boldsymbol{\varepsilon}_{p}(\boldsymbol{x},t) = -v'(z,t)\mathbf{P}_{\boldsymbol{k}} \tag{81}$$

where we used the notation $'=\partial_z$. The corresponding elastic strain can be then written in the form

$$\boldsymbol{\varepsilon}_{e}(\boldsymbol{x},t) = (v'(z,t) + \epsilon_{\tau}(t))\mathbf{P}_{\boldsymbol{k}} + u'(z,t)\boldsymbol{k} \otimes \boldsymbol{k}. \tag{82}$$

Note next that due to the imposed kinematic constraint (79), the elastic stress tensor also has a special structure

$$\boldsymbol{\sigma} = \sigma_{\tau}(z, t)\mathbf{P}_{k} + \sigma_{z}(z, t)\boldsymbol{k} \otimes \boldsymbol{k}$$
(83)

where σ_{τ} is in-plane component and σ_{z} is the normal, axial component. The off-diagonal stresses are clearly absent in our simplified setting, while in-plane stresses have equal radial and hoop components, $\sigma_{r} = \sigma_{\vartheta} = \sigma_{\tau}$.

In what follows we neglect body forces $(\boldsymbol{b}=0)$ and we assume that on the deposition/growth surface (with normal $\boldsymbol{n}\equiv\boldsymbol{k}$) tractions are hydrostatic

$$\boldsymbol{s} = s_n \boldsymbol{n}. \tag{84}$$

On the sliding walls of the cylindrical piston (with normal e_r) tractions that are compatible with our other assumptions are necessarily radial,

$$\mathbf{s} = s_w \mathbf{e}_r. \tag{85}$$

We assume that the functions $s_n(\psi)$ and $s_w(\psi)$ are prescribed and their magnitudes depend on the position of the growth surface. We can now write

$$\sigma_z(\psi(t), t) = s_n(\psi(t)) \tag{86}$$

where

$$\sigma_z = (2\mu + \lambda)u' + 2\lambda(v' + \epsilon_\tau). \tag{87}$$

On the other hand, in view of the constrained kinematics (79), the loading in the transverse direction should be understood in the averaged (integral) form [16]. Specifically we have effectively assumed that

$$\int_0^{\psi(t)} \sigma_\tau(z,t) dz = \psi(t) s_w(\psi(t))$$
(88)

where

$$\sigma_{\tau} = \lambda u' + 2(\mu + \lambda)(v' + \epsilon_{\tau}). \tag{89}$$

We can then conclude that the function $s_w(\psi)$ represents the averaged lateral tractions exerted on the body by the surrounding rigid loading device, see Fig.3. For instance, in the case $s_w = 0$, Eq. (88) represents a continuous analogue of the condition (21), which we used to describe the absence of lateral loading on a discrete stack of unevenly pre-stretched layers.

To characterize our active "agents", we make the matching assumptions regarding the structure of the bulk and surface "generalized forces" featured in the expression of external power (42). Specifically, the corresponding tensor fields are assumed to be of the form:

$$\mathbf{B}_{a}(\mathbf{x},t) = B_{a}(z,t)\mathbf{P}_{k}, \qquad \boldsymbol{\sigma}_{a}(\mathbf{x}) = \sigma_{a}(z,t)\mathbf{P}_{k}$$
(90)

where $B_a(z,t)$ and $\sigma_a(z,t)$ are externally prescribed scalar fields representing microscopically applied sub-continuum controls.

4.2. Evolution equations

Our analysis will be performed under the assumption that mechanical equilibrium holds for macro-displacements in the sense that (44),(45) hold throughout the whole process of crystal growth. We assume further that $\alpha > 0$ in (46) and $\beta > 0$ in (48), while we set $\gamma = 0$ in (47).

In view of the assumptions made above, the mechanical macro-equilibrium in the axial direction for $\sigma_z(z,t)$ takes the form

$$\sigma_z' = 0 \qquad z \in (0, \psi(t)) \tag{91}$$

while the only macro-equilibrium equation involving $\sigma_{\tau}(z,t)$ is (88). The evolution equation for v(z,t) in the bulk reduces to

$$\sigma_{\tau}' + B_a = \alpha \dot{v} \qquad z \in (0, \psi(t)). \tag{92}$$

Note that the dynamics described by (92) terminates at micro-equilibrium where $\sigma'_{\tau} = -B_a$. This suggests an interpretation of B_a as a force of dry friction type preventing the infinitesimal neighboring layers from relative horizontal sliding. For instance, if the tangential stress σ_{τ} is discontinuous across a planar surface z = a so that $\sigma_{\tau}(z) = \sigma_{\tau}^{-} + (\sigma_{\tau}^{+} - \sigma_{\tau}^{-})H(z - a)$, where H(z) is the Heaviside function and σ_{τ}^{\pm} are given constants, the implied micro-equilibrium is reached for $B_a = (\sigma_{\tau}^{-} - \sigma_{\tau}^{+})\delta(z - a)$ where δ is the Dirac delta. The corresponding "generalized force" $\mathbf{B}_a = B_a \mathbf{P}_k$ is then represented by a singular tensor field of the type discussed in [62, 63, 64, 65].

To simplify further the treatment, we now assume that $\alpha = \infty$ which means that v(z,t) = v(z). The corresponding micro-displacement field is then effectively "frozen" at the instant of deposition. Such "freezing" must be, of course, supported by a distribution of the generalized forces $B_a(z)$ which would then provide an effective "shear glue" needed to maintain the acquired level incompatibility.

Given our assumptions, the dynamic equation governing the evolution of the function $\psi(t)$ takes the form

$$W_a - \overline{W} + s_n \overline{u'} + 2\sigma_a \overline{v'} = \beta \dot{\psi}(t) \tag{93}$$

where we continue to use the notation

$$\overline{A}(\mathbf{x}) = A(\mathbf{x}, \vartheta(\mathbf{x})). \tag{94}$$

We re call that in (93), the function $s_n(\psi)$ prescribes a (passively) controlled axial traction. Instead, the control function $\sigma_a(\psi)$ can be viewed as characterizing the active "agents" at the phase boundary, see Fig.3. The function $W_a(\psi)$, formally defined in our general theory as the energy of the incoming material, can be interpreted in the present case of crystallization from a melt as the energy density of the liquid phase at the instant of deposition. Since the liquid phase is loaded hydrostatically by the pressure P, and therefore $s_n = -P$, the simplest assumption would be that the arriving liquid has the same energy density as the corresponding solid loaded hydrostatically by the same pressure P. Under this assumption

$$W_a = \frac{3(1-2\nu)}{2E}P^2 \tag{95}$$

where we have introduced the Young modulus E and the Poisson ratio ν , related to Lamé constants through

$$\mu = \frac{E}{2(1+\nu)}, \qquad \lambda = \frac{E\nu}{(1+\nu)(1-2\nu)}.$$
 (96)

The function W in (93), describing the elasticity of the solid phase, has a standard form

$$W = \mu(2e_{\tau}^2 + e_z^2) + \frac{\lambda}{2}(2e_{\tau} + e_z)^2$$
(97)

where for the tangential and axial components of the elastic strain, we substitute $e_{\tau} = v' + \epsilon_{\tau}$ and $e_z = u'$, respectively. The chosen representation of the energy of the solidifying liquid in (95) is, of course, highly schematic, as it completely neglects the existence of an energy well corresponding to the liquid phase (see, for instance, [66]). Nevertheless, as we show below, even such a simplified formulation is sufficient to illustrate the influence of the micro-mechanical controls encoded in the function $\sigma_a(\psi)$.

4.3. Solution of the dynamic equations

We begin by writing the full system of dynamic equations for the four unknowns functions $u(z,t),v(z),\psi(t),\epsilon_{\tau}(t)$. It includes the equilibrium equations in the bulk:

$$z \in (0, \psi(t)): \begin{cases} \sigma'_z = 0\\ \int_0^{\psi(t)} \sigma_\tau(z, t) dz = \psi(t) s_w(\psi(t)) \end{cases}$$

$$(98)$$

supplemented by the constitutive equations in the bulk

$$z \in (0, \psi(t)): \begin{cases} \sigma_{\tau} = \lambda u' + 2(\mu + \lambda)(v' + \epsilon_{\tau}) \\ \sigma_{z} = (2\mu + \lambda)u' + 2\lambda(v' + \epsilon_{\tau}) \end{cases}$$
(99)

together with the boundary-initial conditions conditions

$$\begin{cases}
\psi(0) = \psi_0 \\
u(0,t) = 0 \\
v(0,t) = v_0 \\
\overline{\sigma}_z(\psi(t),t) = s_n(\psi(t)) \\
\overline{\sigma}(\psi(t),t) = \sigma_a(\psi(t)).
\end{cases}$$
(100)

Here ψ_0 is the thickness of an initial basal layer which is instantaneously created under zero passive and active loading; v_0 is the initial value of the microdisplacement parameter at deposition. Since we deal with a free boundary problem, we must include the evolution equation for the deposition/growth surface:

$$z = \psi(t): \quad W_a - \overline{W} + s_n \overline{u'} + 2\sigma_a \overline{v'} = \beta \dot{\psi}(t).$$
 (101)

We assume that the parameters ψ_0 , v_0 , $W_a(P)$ and the control functions $s_n(\psi)$, and $s_w(\psi)$ are all prescribed, however, as we show below, they cannot be chosen completely arbitrarily.

Substituting (99) and (100)_{4,5} into (98) we immediately obtain an explicit representation of the "frozen" micro-displacements characterized by the function v(z)

$$v'(z) = -\frac{1-\nu}{E} \left(s_w(z) - \sigma_a(z) + \mathcal{F}(z) \right)$$
 (102)

where we have introduced the auxiliary function

$$\mathcal{F}(z) = \int_0^z \frac{s_w(\tilde{z}) - \sigma_a(\tilde{z})}{\tilde{z}} d\tilde{z}.$$
 (103)

To avoid the formation of a singularity at z=0, the function $\mathcal{F}(z)$ must remain bounded as $z\to 0$; physically, this means that the controls should be applied sufficiently gradually. It is also clear from (103) that in the special case when the passive axial forces and the active lateral forces on the deposition surface are equal

$$\sigma_a(\psi) = s_w(\psi) \tag{104}$$

the micro-displacements are absent and, in particular, no incompatibility is generated during the process. Moreover, one can see that v'=0 if and only if $s_w(z) - \sigma_a(z) = c/z$ for some constant c, so to avoid a stress singularity at the origin we must necessarily have c=0. Consequently, a microscopically engineered active deposition protocol satisfying (104) can be termed *compatible*, as it ensures that any solid body grown under these conditions is stress-free when passive tractions are removed.

Given our simplifying assumptions, we can also find explicit expressions for the transversal strain ${\bf r}$

$$\epsilon_{\tau}(t) = \frac{(1-\nu)}{E} \left(\mathcal{F}(\psi(t)) + s_w(\psi(t)) - \frac{\nu}{(1-\nu)} s_n(\psi(t)) \right)$$
(105)

and for the axial strain

$$u'(z,t) = \frac{1}{E(\nu-1)} \left((1+\nu)(2\nu-1)s_n(\psi(t)) + 2E\nu(v'(z) + \epsilon_\tau(t)) \right)$$
 (106)

where it is implied that $z \leq \psi(t)$ while the function $\psi(t)$ is determined from (93).

4.4. Regime diagram

Let us now consider a special case in which the role of different deposition strategies can be assessed quantitatively. To begin with, in order to avoid the formation of a singularity at z=0, we divide the deposition process into two stages: a "nucleation" stage, during which an initial layer of thickness ψ_0 is instantaneously created under zero loading, and therefore

$$\begin{cases} s(z) = 0 \\ \sigma_a(z) = 0 \\ s_w(z) = 0 \end{cases}$$
 (0 < z < \psi_0) (107)

and a "growth" stage when the crystalization advances under special loading conditions (see Fig.3)

$$\begin{cases} s(z) = -P \\ \sigma_a(z) = -P_a \\ s_w(z) = -P_w \end{cases} (\psi_0 < z). \tag{108}$$

In what follows, it will be convenient to use dimensionless parameters

$$p_a = P_a/P, \qquad p_w = P_w/P \tag{109}$$

with the goal of constructing a regime diagram in the (p_a, p_w) space. Within this setting, we have $\mathcal{F}(z) = 0$ during the "nucleation" stage, and

$$\mathcal{F}(z) = P(p_a - p_w) \log(z/\psi_0) \tag{110}$$

during the "growth" stage. The evolution of the phase boundary $\psi(t)$ is determined by solving the problem

$$\begin{cases} \beta \dot{\psi}(t) = \mathcal{G}(\psi(t)) \\ \psi(0) = \psi_0 \end{cases} \tag{111}$$

where

$$\mathcal{G}(\psi) = 2p_a(1-\nu)\frac{P^2}{E}\left(A + (p_a - p_w)\log\left(\frac{\psi}{\psi_0}\right)\right). \tag{112}$$

In (111) we also introduced the notations

$$A = \frac{S(\nu)}{2p_a} + \frac{p_a - 2p_w}{2}, \qquad S(\nu) = \frac{2 - 3\nu}{1 - \nu}.$$
 (113)

Note first that the ODE (111) has a single fixed point

$$\psi_e = \psi_0 e^{A/(p_w - p_a)} \tag{114}$$

where $\mathcal{G}(\psi_e) = 0$. It is stable if

$$\mathcal{G}'(\psi_e) = \frac{2P^2}{E\psi_e} p_a (1 - \nu)(p_a - p_w) < 0 \tag{115}$$

or, equivalently, if

$$p_w > p_a. (116)$$

We recall from (104) that the limiting case $p_w = p_a$ corresponds to *compatible* growth.

We are now in a position to identify distinct dynamic regimes in the parameter plane (p_a, p_w) (see Fig. 4). Specifically, we observe stable growth $(\psi_0 < \psi_e < +\infty)$ in region 1, where $p_w > p_a$ and A > 0, and therefore in terms of the parameters:

$$\frac{1}{2} \left(\frac{S(\nu)}{p_a} + p_a \right) > p_w > p_a. \tag{117}$$

In region 2, where $p_w > p_a$ and A < 0 so that

$$p_w > \max\left(\frac{1}{2}\left(\frac{S(\nu)}{p_a} + p_a\right), p_a\right) \tag{118}$$

we observe stable resorption $(0 < \psi_e < \psi_0)$. Regions 3 (where A > 0 and $p_a > p_w$) and 4 (where A < 0 and $p_a > p_w$) correspond to unstable regimes, because in both cases $\mathcal{G}'(\psi_e) > 0$.

We now discuss in more detail two special regimes, emphasizing the role played by the microscopically generated control, represented by the active tangential stress $\sigma_a = -p_a P$.

• Compatible (elastic) growth. This is the classically studied regime with no prestress accumulated in the body, see the line $p_a = p_w$ in Fig.4(a). In this case the fixed point (114) becomes degenerate, as it is displaced either to infinity or to zero depending on whether A > 0 or A < 0, respectively. Specifically, when

$$p_a = p_w < \sqrt{S(\nu)} \tag{119}$$

the function $\psi(t)$ blows-up with time. Instead, it collapses to zero when

$$p_a = p_w > \sqrt{S(\nu)}. (120)$$

The critical threshold $p_a = p_w = \sqrt{S(\nu)}$ will then define a boundary between unbound growth and full resorption. One can see that the presence of the microscopic mechanical activity can, in principle, reverse the direction of a phase transformation from solidification to melting.

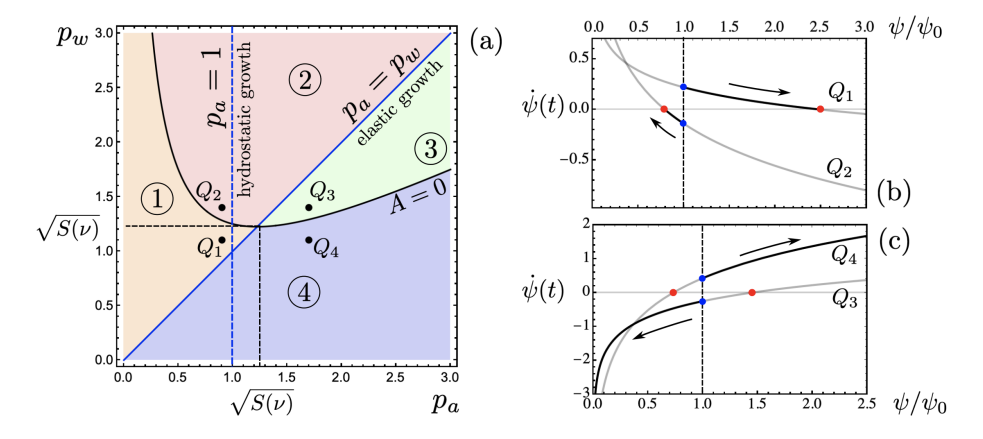
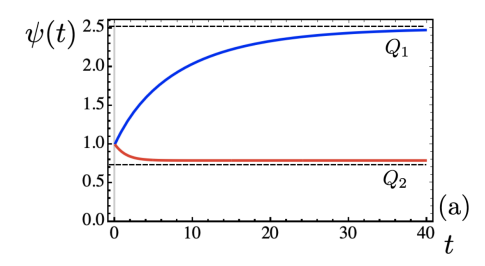


Figure 4: (a) Regime diagram in the space of parameters (p_a, p_w) for the evolution problem $\dot{\psi} = \mathcal{G}(\psi)$ with $\psi(0) = \psi_0$, see (111). In regions 1 and 2, $\mathcal{G}'(\psi_e) < 0$, producing asymptotically stable regimes. In regions 3 and 4, $\mathcal{G}'(\psi_e) > 0$, indicating unstable regimes. (b)–(c) The trajectories of interest on the phase plane $(\dot{\psi}, \psi/\psi_0)$. Here ψ_0 is the initial location of the growth surface (blue dot). (b) Stable trajectories (regions 1 and 2) converge asymptotically to equilibria (red dots), which are either above (Q_1) or below (Q_2) the initial state. (c) Unstable trajectories (regions 3 and 4) either extending to infinity (Q_4) or collapsing to zero (Q_3) . All plots are obtained with Poisson ratio $\nu = 0.3$. The choices of the parameters P, E, p_a, p_w only contribute to rescaling of the trajectories shown in (b) and (c).

Note that while the *compatible* phase transformation paradigm, already employed by Gibbs in his classical study of solid-liquid interface stability [47], is an analytically transparent choice, it is likely a useful abstraction rather than a physically realizable mechanism. Indeed, to avoid the emergence of incompatibility under the assumption of *compatible* growth, the hydrostatically stressed liquid elements must be transformed into non-hydrostatically stressed solid elements by some physically obscure active "agents" executing the required prestretch. In this perspective the development of at least some incompatibility appears physically more natural, in particular, given the random orientation of the crystallites during the solidification from a melt. We also observe that *compatible* growth does not allow the system to attain a configuration of finite size: this limitation becomes a crucial obstacle when applying the model to biological systems, where, interestingly, the connection between the emergence of finite-sized configurations and the inherently incompatible nature of growth has been recognized (see, e.g., [67, 68]).

• Hydrostatic growth. Another important regime is characterized by the condition $\sigma_a = s_n = -P$, represented by the line $p_a = 1$ in Fig. 4, and describing a situation where the arriving solid elements are loaded exactly as their parent fluid elements. In this case the active micro stresses match their passive macroanalogs, ensuring that the deposited elements are loaded hydrostatically. One can say that the liquid retains the memory of its stress state as it transforms into the solid. While such an assumption seems natural [18, 15], it clearly leads to the development of incompatibility and accumulation of residual stresses.



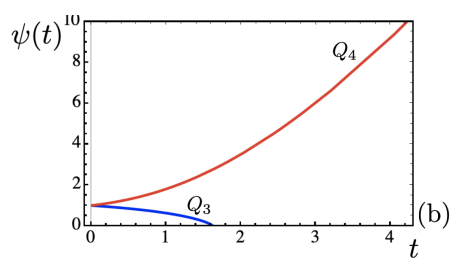


Figure 5: (a) Evolution of growing surfaces $\psi(t)$ represented by the solutions of the problem $\dot{\psi} = \mathcal{G}(\psi)$ with initial condition $\psi(0) = 1$, and parameters corresponding to the points $Q_1 = (0.9, 1.1)$ and $Q_2 = (0.9, 1.4)$ in Fig. (4). In both cases, $\psi(t)$ converges to a finite equilibrium, which is higher than the initial value in the first case (solidification) and lower in the second (melting). (b) Behavior of the function $\psi(t)$ corresponding to points $Q_3 = (1.7, 1.4)$ and $Q_4 = (1.7, 1.1)$ in Fig. (4). In these cases, no stabilization is possible: $\psi(t)$ collapses to zero in the former case, while it blows up in the latter case. Parameters are fixed at $\nu = 0.3$ and P = E = 1.

By implementing the hydrostatic growth protocol, different dynamic regimes can be reached depending on the value of the parameter p_w , describing the lateral pressure on the walls of the cylinder. When $p_w < 1$ (lateral pressure is lower than the liquid pressure), the solid phase grows indefinitely. When $p_w \in (1, 2 + 0.5/(\nu - 1))$, the system evolves toward a stable equilibrium size which exceeds the initial one (solidification). When instead $p_w > [2 + 0.5/(\nu - 1)]$, the stabilization produces system shortening (melting). These observations explain, for instance, the peculiar behavior observed during ice melting, as reported in [69].

The obtained results are also relevant for the description of multicellular tumor spheroids [70], where lateral confinement, known as "stress clamping" (quantified by parameter analogous to p_w), was shown to slow down growth and even trigger resorption. Similar mechanically mediated regulation of growth has also been documented for healthy tissues [71, 72].

4.5. The final configuration

The presence of accumulated incompatibility can be detected by residual stresses in the final configuration. In the absence of applied macroscopic tractions, the equilibrium equations can be solved analytically, revealing that the residual stresses in a cylinder of the final height ψ_f are of the form

$$\sigma_z^0 = 0, \qquad \sigma_\tau^0(z) = \frac{E}{1 - \nu} \left(\langle \gamma \rangle - \gamma(z) \right)$$
 (121)

where

$$\gamma(z) = -v'(z) \tag{122}$$

is the tangential component of the inelastic strain (81) while

$$\langle \gamma \rangle = \frac{1}{\psi_f} \int_0^{\psi_f} \gamma(z) dz \tag{123}$$

stands for the average accumulated inelastic strain. Note an analogy between (121) and the corresponding result in our discrete theory (20).

The representation (121) suggests that, in the kinematically constrained case under consideration, a natural measure of incompatibility is

$$\eta(z) = \langle \gamma \rangle - \gamma(z) = v'(z) - \frac{v(\psi_f) - v(0)}{\psi_f}.$$
 (124)

Noting from (124) that linear distributions of micro-displacements v(z) are always compatible in this sense, we introduce the "compatible component" of the micro-displacement field

$$v_c(z) = v(0) + \frac{z}{\psi_f} (v(\psi_f) - v(0))$$
 (125)

which allows us to isolate the "incompatibility-related" component

$$v_i(z) = v(z) - v_c(z) \tag{126}$$

which is characterized by the property

$$\eta(z) = v_i'(z). \tag{127}$$

Furthermore, because by definition $v_i(0) = v_i(\psi_f) = 0$, it is clear that $\eta(z) = 0$ if and only if $v_i(z) = 0$.

Observe next that using these new definitions, we can rewrite the expression for the final elastic strain in the grown solid (82) in the form

$$\varepsilon_e(\mathbf{x}) = \nabla \hat{\mathbf{u}}(\mathbf{x}) + v_i'(z)\mathbf{P}_k, \qquad \hat{\mathbf{u}}(\mathbf{x}) = u(z)\mathbf{k} + r\hat{\epsilon}_{\tau}\mathbf{e}_{\tau}$$
 (128)

where we have set

$$\hat{\epsilon}_{\tau} = \epsilon_{\tau} - \langle \gamma \rangle = (P/E) \left(\nu - p_w (1 - \nu) \right). \tag{129}$$

The message behind such a rewriting is that the uniform lateral micro-dilatation can be absorbed into macro-deformation, which is similar to what happens in the discrete case already, see for instance Eq. (21).

To compute the distribution of incompatibility $\eta(z)$ when the body reaches the final size with $\psi(T_f) = \psi_f > \psi_0$, we first introduce useful notations. Suppose that the function $\gamma(z)$ is defined by (122). We use the superscript "—" for the "nucleation" layer at $z \in (0, \psi_0)$ where $\gamma(z) = \gamma^-(z) = 0$. Accordingly, we identify by the superscript "+" the "grown" layer at $z \in (\psi_0, \psi_f)$ where $\gamma(z) = \gamma^+(z) \neq 0$.

Note next that from $v^-(0) = 0$ we obtain $v^-(z) = 0$ in $(0, \psi_0)$, and by integrating (102) with initial condition $v^+(\psi_0) = 0$, we obtain $v^+(z)$ in (ψ_0, ψ_f) . More specifically, we obtain

$$v_i^-(z) = 0, \qquad v_i^+(z) = \frac{P(p_w - p_a)(1 - \nu)}{E} z \log\left(\frac{z}{\psi_f}\right).$$
 (130)

The corresponding incompatibility takes the form

$$\eta^{-}(z) = 0, \qquad \eta^{+}(z) = \frac{P(p_w - p_a)(1 - \nu)}{E} \left(1 + \log\left(\frac{z}{\psi_f}\right) \right).$$
(131)

To obtain the distribution of macro-displacements we need to integrate (106) in $(0, \psi_0)$ with the boundary condition $u^-(0, T_f) = 0$, giving

$$u^{-}(z, T_f) = Pz \frac{2p_w \nu - 1 + 2(p_w - p_a)\nu \log(\psi_f/\psi_0)}{E}.$$
 (132)

and also (106) in (ψ_0, ψ_f) with the boundary condition $u^-(\psi_0, T_f) = u^+(\psi_0, T_f)$, giving

$$u^{+}(z, T_f) = Pz \frac{2p_w \nu - 1 + 2\nu(p_a - p_w)\log(z/\psi_f)}{E}.$$
 (133)

The functions $u^{\pm}(z,T)$ and $v_i^{\pm}(z)$ are illustrated in Fig.6(b).

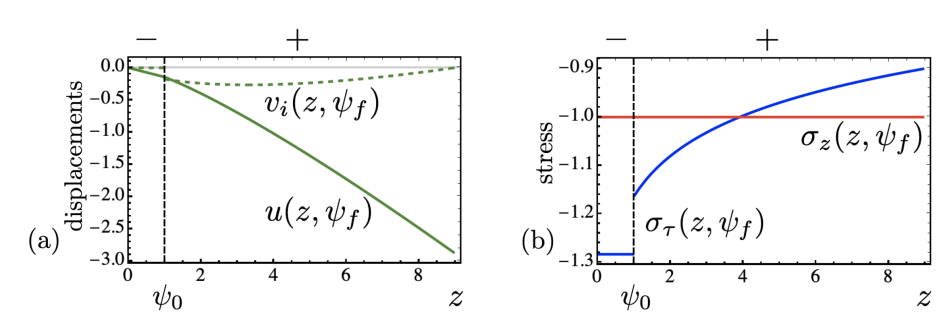


Figure 6: (a) Macro displacement field (solidline) and incompatible-micro displacement field (dashedline); (b) stress components in the axial direction (σ_z) and in the horizontal direction (σ_τ), in the basal layer "-" (0, ψ_0) and in the grown region "+" (ψ_0 , ψ_f). Here $\psi_0 = 1$, $\nu = 0.3$, P = E = 1, and we have chosen (p_a, p_w) corresponding to point Q_1 in Fig.4.

It is also instructive to reconstruct the final stress configuration. Thus, in the "nucleation" zone

$$z \in (0, \psi_0): \begin{cases} \sigma_z^-(z, T_f) = -P \\ \sigma_\tau^-(z, T_f) = -P \left(p_w + (p_a - p_w) \log \left(\psi_0 / \psi_f \right) \right) \end{cases}$$
(134)

while in the "grown" zone

$$z \in (\psi_0, \psi_f): \qquad \begin{cases} \sigma_z^+(z, T_f) = -P \\ \sigma_\tau^+(z, T_f) = -P \left(p_a + (p_a - p_w) \log(z/\psi_f) \right). \end{cases}$$
(135)

Both distributions are illustrated in Fig. 6(a). Observe that the axial stress σ_z is uniform, which is consistent with the statically determined nature of the problem along the axial direction. In contrast, the tangential (horizontal) stress σ_τ is inhomogeneous as long as $p_a \neq p_w$. Note also a tangential stress discontinuity across the internal interface at $z = \psi_0$. When $p_a = p_w$, the stress distribution becomes homogeneous throughout the entire body even when the configuration is non-hydrostatic, which is the behavior anticipated by Gibbs [47] in the absence of incompatibility.

4.6. Discussion

Our analysis of a non-hydrostatically loaded solid in contact with its melt presented in this section can be viewed as an extension of Gibbs seminal study [47]. Here we discuss the new elements contributed by our approach to the established picture of this phenomenon.

While chemical aspects such as compositional differences between the coexisting solid and liquid phases, and the associated heat release, have been disregarded, we have proposed a more nuanced representation of the solid phase compared to previous studies. In addition to the elastic strain, we now also account for inelastic contributions; furthermore, we introduce a mechanism that regulates the strain incompatibility arising during solidification, by incorporating a description of the microscopic activity responsible for imposing pre-stress on the newly formed solid elements.

We recall that in Gibbs' classical treatment [47], the growth of the solid phase from its melt was effectively assumed to be compatible, or equivalently, purely elastic (see also [49, 48, 66]). In contrast, our study focuses on the emergence of incompatibility enabled by an extended set of controls, involving the interplay among three quantities: the classical traction exerted by the fluid phase, s = -P (the macroscopic axial stress); the lateral pressure, $s_w = -p_w P$ (the macroscopic lateral confinement stress); and the active surface (tangential) stress, $\sigma_a = -p_a P$. In these terms, Gibbs implicitly assumed that $p_a = p_w$, or equivalently, $\sigma_a = s_w$.

Our approach reveals a much broader repertoire of solidification scenarios compared to the conventional picture limited to compatible growth, which is represented by a marginally stable dividing line in Fig. 4. Under our expanded set of controls, the entire $p_a - p_w$ plane becomes accessible, allowing for a range of growth pathways and stability regimes which may be of particular relevance for living systems that are known to experience biologically functional liquid-solid transitions. In particular, microscale mechanical activity represented by the deposition pressure p_a was shown to be a crucial player, able by itself to both initiate and inhibit growth. It was also shown that bounded and unbounded growth occur depending on whether the parameters (p_a, p_w) fall into the corresponding regions in the phase diagram shown in Fig.4.

In this respect, we recall that in his study, Gibbs observed that in the typical case of compatible growth with $p_w \neq 1$ (i.e., $s_w \neq -P$), even thermodynamically equilibrated solid-liquid interface is morphologically unstable. More generally, he concluded that a non-hydrostatically stressed solid in equilibrium with a hydrostatically stressed fluid is inherently unstable: his argument was that a stressed element of the solid surface can always dissolve into the fluid/melt and recrystallize elsewhere in hydrostatic conditions, thereby lowering the total energy. This instability mechanism was later examined more systematically in [73] in a linearized setting, and in [74] within a geometrically and physically nonlinear framework. More recently, it was shown that the same instability can also be detected by using a novel equilibrium jump condition discovered in [75]. Translated into our language, this condition states that under the assumption

of elastic growth with $p_a=p_w$, stable coexistence of a solid with a fluid is only possible when $p_w=1$, that is, when the solid is hydrostatically stressed. Here we broaden the stability picture developed by Gibbs and his successors by allowing for inelastic growth, and we show that, in this case, stability may in principle be recovered even when $p_w \neq 1$, due to the presence of active "agents" able to impose a non-classical micro-stress σ_a at the deposition surface.

We also mention that while the final size ψ_e reachable in the solidification process is ultimately selected dynamically, our analysis suggests that it depends only on the initial size of the body ψ_0 . In other words, in contrast to models where growth leads to an intrinsic size selection, see for instance [67, 68]), here due to the absence of an internal length scale, we observe only a finite size effect. An important observation, however, is that the ultimate stabilization takes place only when $p_w \neq p_a$, that is, when growth is incompatible. Instead, as we have seen, along the compatibility line $p_w = p_a$, no such final stabilization occurs as the system either explodes or collapses.

To summarize, despite the simplifying assumptions made in our study, in particular the fact that we focus exclusively on mechanical aspects, we have provided a compelling evidence that the formation of incompatibility is an essential part of solidification, with inelastic strains playing a fundamental role on the stability of the solid-liquid front. A natural conjecture emerging from our study is that the realistic self-driven solidification process can be hardly "elastic" and therefore the emergence of inelastic strains and the formation of incompatibility in such process is unavoidable. The effective nature of active controls in a constrained cooling process remains to be understood through detailed microscopic studies, see for instance [76, 77, 78, 79, 80]. A comprehensive mechanical study of the solidification process in realistic technological systems accounting for the formation of residual stresses is also an important open problem, despite many past and ongoing efforts [81, 82, 83, 84, 85].

5. Winding with pre-stretch

Our second example concerns the technologically important problem of roll winding, where residual stresses arise rather naturally due to variable tension applied to a wire, a tape or a film [14]. The challenge is to link the emerging residual stresses to particular winding protocol [25].

Recently, a problem of controlling stress distribution in wound rolls and other similar "grown" structures has received significant attention in the technical literature aimed at the optimization of winding machines [86, 87, 88, 89, 90, 91]. In most of these studies the analysis was performed at what we would interpret as a micro-scale, in particular the thickness of the attached film, tape or wire was explicitly resolved and the emerging incompatibility was represented by the relative slip of the attached layers.

Our coarse grained approach offers a possibility to describe the same winding processes directly at the macro-scale, without the layering thickness explicitly resolved. In such approach, winding is interpreted as a surface deposition pro-

cess, with the variable tension on the deposited segment of tape, wire or film being responsible for the emerging incompatibility.

5.1. Problem setting

We assume for simplicity that the winding process is two-dimensional, taking place around a cylindrical core. The grown body is then a hollow disk that remains confined to a plane, see Fig.7. At the micro-scale, winding can be described as sequential addition of pre-stressed thin strips of thickness h to a growing core region. A controlled tangential pulling force is applied on each individual segment (strip) as it adheres to the growing core.

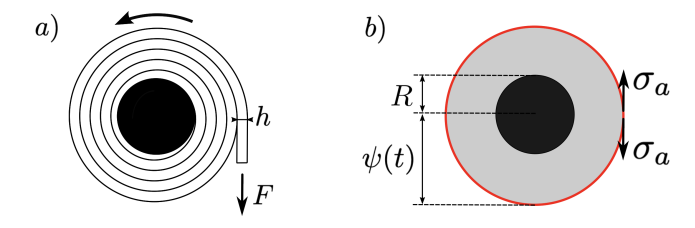


Figure 7: a) Representation of the winding process in the discrete setting, with a layer of thickness h is added to the coil with a pulling force F applied. b) Continuous representation of the same process under the assumption that $h \to 0$ and $F \to 0$, while the ratio $\sigma_a = F/h$ remains finite. Winding starts off from an internal rigid core of radius R, with externally controlled current placement of the growth surface $\psi(t)$ (red line).

Denote by F the tangential pulling force and suppose that in the macroscopic approach we are dealing with the limit $h \to 0$ and $F \to 0$, with the ratio $\sigma_a = F/h$ remaining finite, see Fig.7. The task of developing an adequate macroscopic continuum model of winding is assisted by the fact that, in contrast to the case of solidification, we have access to a physically transparent micromodel operating with finite values of parameters h and F.

For consistency with the microscopic picture, we assume that in the macroscopic continuum formulation the body is growing radially while preserving cylindrical symmetry. We also assume for simplicity that post-deposition slips between the neighboring strips are prohibited, allowing us to use the limit of "frozen" inelastic strain $\varepsilon_p(x)$. As another simplification, we also prescribe the function $\vartheta(x)$ that describes the location of the deposition surface. To summarize, roll winding in our formulation is viewed as a process where the acquired incompatibility is controlled by the radial winding velocity D(t) and by the tangential pulling force $\sigma_a(r,t)$.

An important goal of our analysis will be to compare two solutions of the formulated problem. One of them, is a purely macroscopic solution obtained by solving incremental equilibrium equations outlined in Sec. 3.4 and by making no explicit reference to micro-displacements. Another one, is a solution of the full boundary value problem involving micro- and macro-displacements as formulated in Sec. 3.1. Such comparison is possible because our formula-

tion of the winding problem is compatible with the decoupling of micro- and macro-evolutions.

5.2. Macroscopic approach

For additional analytical transparency we ignore space and time dependency of the controls and we assume that

$$D(t) \equiv D, \qquad \sigma_a(r, t) \equiv \sigma_a$$
 (136)

where D and σ_a are given constants. In particular, this means that the growth radius evolves according to $\psi(t) = R + Dt$, where R denotes the initial radius of the coil, interpreted as a rigid mandrel. The function $t = \vartheta(r)$ representing the time when the deposition surface is at the radial distance r, is obtained by inverting $\psi(t)$, giving (see Fig.7)

$$\vartheta(r) = (r - R)/D. \tag{137}$$

Because winding takes place under null macroscopic loading, while the microscopic pulling force is purely tangential, we conclude that on the deposition surface

$$s_n(\psi(t)) = 0, \qquad \sigma_\tau(\psi(t), t) = \sigma_a.$$
 (138)

Note next that because loading is radially symmetric, the incremental displacements are purely radial,

$$\dot{\boldsymbol{u}}(r,t) = \dot{\boldsymbol{u}}(r,t)\boldsymbol{e}_r \tag{139}$$

where e_r is the radial unit vector and the superposed dot indicates differentiation with respect to time, $\dot{u} = \partial u/\partial t$. The resulting incremental strain is

$$\dot{\boldsymbol{\varepsilon}}(r,t) = \dot{\epsilon}_r(r,t)\boldsymbol{e}_r \otimes \boldsymbol{e}_r + \dot{\epsilon}_{\theta}(r,t)\boldsymbol{e}_{\theta} \otimes \boldsymbol{e}_{\theta}$$
 (140)

where e_{θ} is the angular unit vector and we introduced notations $\dot{\epsilon}_r = \dot{u}'$, and $\dot{\epsilon}_{\theta} = \dot{u}/r$, where superposed apex now indicates differentiation with respect to radial distance, $u' = \partial u/\partial r$.

The incremental Cauchy stress is then

$$\dot{\boldsymbol{\sigma}}(r,t) = \dot{\sigma}_r(r,t)\boldsymbol{e}_r \otimes \boldsymbol{e}_r + \dot{\sigma}_{\theta}(r,t)\boldsymbol{e}_{\theta} \otimes \boldsymbol{e}_{\theta} \tag{141}$$

where σ_{θ} is the the hoop stress representing in this setting the surface stress σ_{τ} . Because according to our assumptions, inelastic strains are frozen at the moment of deposition, the incremental linear elastic constitutive relations take the form

$$\dot{\sigma}_{r/\theta} = 2\mu \dot{\epsilon}_{r/\theta} + \lambda (\dot{\epsilon}_r + \dot{\epsilon}_\theta). \tag{142}$$

Note that in (142) we used the 2D Lamé coefficients (λ, μ) , that are related to the corresponding 2D elastic modulus E and the 2D Poisson coefficient ν through the relations $\mu = E/(2(1+\nu))$ and $\lambda = \nu E/(1-\nu^2)$.

5.2.1. Incremental problem

As in the general case discussed in Sec.3.4 we can write the incremental equilibrium equation in the form

$$Div\dot{\boldsymbol{\sigma}} = \mathbf{0} \tag{143}$$

which in the presence of radial symmetry reduces to

$$\dot{\sigma}_r' + (\dot{\sigma}_r - \dot{\sigma}_\theta)/r = 0. \tag{144}$$

The resulting mathematical problem for the unknown field $\dot{u}(r,t)$ takes the form

$$\begin{cases}
\dot{\varepsilon}_r = \dot{u}' \\
\dot{\varepsilon}_{\theta} = \dot{u}/r \\
\dot{\sigma}_{r/\theta} = 2\mu\dot{\varepsilon}_r + \lambda(\dot{\varepsilon}_r + \dot{\varepsilon}_{\theta}) \\
\dot{\sigma}'_r + (\dot{\sigma}_r - \dot{\sigma}_{\theta})/r = 0.
\end{cases} (145)$$

To obtain the boundary condition on the deposition surface we need, like we did more in general in (73), to take the divergence of the surface stress

$$\overline{\sigma}(x) = \sigma(x, \vartheta(x)) \tag{146}$$

which gives the condition

$$\dot{\boldsymbol{\sigma}}\boldsymbol{n} = D\operatorname{Div}\overline{\boldsymbol{\sigma}}.\tag{147}$$

By specializing (147) to our case, we obtain

$$\dot{\sigma}_r(\psi(t), t) = -D \frac{\sigma_a}{\psi(t)}.$$
(148)

We reiterate that in our setting the parameters D and σ_a as well as the function $\psi(t)$ are assumed to be known. Recall also that in view of (66), the radial displacement can be written in incremental form

$$\tilde{u}(r,t) = \int_{\vartheta(r)}^{t} \dot{u}(r,s) \, ds. \tag{149}$$

Finally, because on the internal surface (the rigid core) we assume that u(R, t) = 0 for all t, the corresponding incremental displacement field must satisfy

$$\dot{u}(R,t) = 0. \tag{150}$$

5.2.2. Solution of the incremental problem

The general solution of the problem (145) is

$$\dot{u}(r,t) = a(t)r + b(t)/r \tag{151}$$

with the unknown functions a(t), b(t) to be obtained from the incremental boundary conditions

$$\dot{u}(R,t) = 0, \qquad \dot{\sigma}_r(\psi(t),t) = -D\sigma_a/\psi(t). \tag{152}$$

After the incremental problem is solved, the final displacement field and the corresponding stress distribution can be recovered (as in Sec.3.4) using (149) together with

$$\sigma_{r/\theta}(r,t) = \bar{\sigma}_{r/\theta}(r) + \int_{\vartheta(r)}^{t} \dot{\sigma}_{r/\theta}(r,s) \, ds. \tag{153}$$

The resulting relations can be written explicitly

$$\tilde{u}(r,t) = \frac{\sigma_a}{2} \frac{(r^2 - R^2)(1 - \nu)}{rE} \log \left(\frac{r^2(1 + \nu) + R^2(1 - \nu)}{\psi(t)^2(1 + \nu) + R^2(1 - \nu)} \right)$$
(154)

$$\sigma_r(r,t) = \frac{\sigma_a}{2} \left(1 + \frac{R^2(1-\nu)}{r^2(1+\nu)} \right) \log \left(\frac{r^2(1+\nu) + R^2(1-\nu)}{\psi(t)^2(1+\nu) + R^2(1-\nu)} \right)$$
(155)

$$\sigma_{\theta}(r,t) = \sigma_a + \frac{\sigma_a}{2} \left(1 - \frac{R^2(1-\nu)}{r^2(1+\nu)} \right) \log \left(\frac{r^2(1+\nu) + R^2(1-\nu)}{\psi(t)^2(1+\nu) + R^2(1-\nu)} \right).$$
 (156)

They are illustrated in Fig.8. In particular, panel (a) shows the distribution of radial and circumferential stress at successive time instants. As expected, the radial stress is always compressive and vanishes at the outer radius, while the circumferential stress is tensile and constant at the outer boundary. Inside the domain, it can be either tensile or compressive. In panel (b), we show the displacement of material points which are always negative as intuitively expected, because during winding the radial compression increases, leading to inward overall motion.

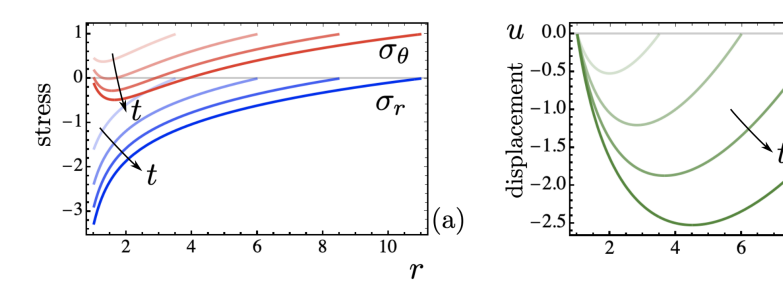


Figure 8: (a) Distribution of radial (σ_r) and hoop (σ_θ) stress components during the winding process advancing according to $\psi(t) = R + Dt$, with prescribed D. (b) Displacement field in the coil during deposition. Parameters: $\sigma_a = E = 1$, R = 1, D = 1, $\nu = 1/3$.

The inelastic strains in the forming coil are obtained from

$$\tilde{\gamma}_{r/\theta}(r) = \epsilon_{r/\theta}(r,t) - e_{r/\theta}(r,t) \tag{157}$$

(b)

where the total strains are $\epsilon_r(r,t) = \tilde{u}'(r,t)$ and $\epsilon_{\theta}(r,t) = \tilde{u}(r,t)/r$ and where the components of the elastic strain are

$$e_{r/\theta} = (\sigma_{r/\theta}(r, t) - \nu \sigma_{\theta/r}(r, t))/E. \tag{158}$$

Using our explicit solution, we finally obtain the components of inelastic strain in the form

$$\tilde{\gamma}_r(r) = \frac{\sigma_a}{E} \frac{r^2(1+\nu) - R^2(1-\nu)}{r^2(1+\nu) + R^2(1-\nu)}, \qquad \tilde{\gamma}_\theta(r) = -\frac{\sigma_a}{E}.$$
 (159)

As expected, the inelastic strains are time independent, and the resulting incompatibility carries both regular and singular contributions. The regular contribution $\eta = \text{CurlCurl}\varepsilon_p$, can be written in our case in the form

$$\boldsymbol{\eta} = \eta(r)\boldsymbol{k} \otimes \boldsymbol{k},\tag{160}$$

where

$$\eta(r) = \tilde{\gamma}_r''(r) + \frac{1}{r} (2\tilde{\gamma}_\theta'(r) - \tilde{\gamma}_r'(r)) = \frac{4R^2(1 - \nu^2)\sigma_a}{E(r^2(1 + \nu) + R^2(1 - \nu))^2}.$$
 (161)

The singular part appears because the domain is non-simply connected. It represents a wedge disclination with the opening angle equal to

$$\Omega_p = 2\pi R \left(\tilde{\gamma}_{\theta}'(R) + \frac{\tilde{\gamma}_{\theta}'(R) - \tilde{\gamma}_{r}'(R)}{R} \right) = -2\pi \frac{1+\nu}{E} \sigma_a$$
 (162)

see [8, 10] for details, where a similar problem was considered.

5.2.3. Compatible component of inelastic strain

It is important to stress that the final distribution of residual stress (155), (156), emerging at the end of the winding process, contains not only incompatible (regular and singular), but also compatible contribution which can be linked to the presence of an external constraint represented by the rigid mandrel.

Indeed, we can show that even after a complete relaxation of the micro-displacement tensor \mathbf{V}_{τ} , as it would be the case if we activate the relaxation process described by (46) with $\mathbf{B}_a = \mathbf{0}$, the grown coil will still support nonzero residual stresses of compatible nature. To determine their structure we need to solve the problem

$$\begin{cases}
\sigma = 2\mu\varepsilon_e + \lambda(\operatorname{tr}\varepsilon_e)\mathbf{I} \\
\operatorname{Div}\boldsymbol{\sigma} = \mathbf{0} \\
\operatorname{Curl}_n\boldsymbol{\sigma} = \mathbf{0}
\end{cases}$$
(163)

where ε_e is viewed as an unknown field. Under the assumption of radial symmetry, the diagonal components of elastic strain (e_r, e_θ) and the corresponding components of stress $(\sigma_r, \sigma_\theta)$ must satisfy the system of equations

$$\begin{cases}
\sigma_{r/\theta} = 2\mu e_{r/\theta} + \lambda(e_r + e_\theta) \\
\sigma_r' + (\sigma_r - \sigma_\theta)/r = 0 \\
\sigma_\theta' + (\sigma_\theta - \sigma_r)/r = 0.
\end{cases}$$
(164)

By straightforward integration we find that

$$e_{r/\theta} = c_1 \pm \frac{c_2}{r^2} \tag{165}$$

where $c_{1/2}$ are integration constants. It is easy to check that such elastic strain field carries neither regular nor singular incompatibility. Their compatible origin is, of course, in line with our discussion in Sec. 3.3.

To identify the compatible component in the final distribution of residual stress (155), (156), we can use linearity of the problem and consider two boundary value problems. In both problems we use the inelastic strains $(\tilde{\gamma}_r, \tilde{\gamma}_\theta)$ acquired at the end of winding, see Eq.(159), as the internal loading.

The first problem, \mathcal{P}_1 , will have the boundary conditions:

$$\begin{cases} \sigma_r(\psi_f) = 0\\ u(R) = 0. \end{cases}$$
 (166)

Since the solution of the ensuing problem describes the configuration of the grown coil the resulting stress distribution coincides with the one represented by (155), (156) with $\psi(t) = \psi_f$.

The second problem, \mathcal{P}_2 , is characterized by different set of boundary conditions:

$$\begin{cases} \sigma_r(\psi_f) = 0\\ \sigma_r(R) = 0 \end{cases}$$
 (167)

and describes the grown coil without the internal mandrel: in this case stresses are solely due to incompatibility.

By solving these two linear problems and then subtracting the corresponding stress distributions we can isolate the contribution to the plastic strains $(\tilde{\gamma}_1, \tilde{\gamma}_2)$ that arises from the rigid core alone. We will refer to it as a solution of the difference problem $\mathcal{P}_0 = \mathcal{P}_1 - \mathcal{P}_2$.

After performing these operations we obtain the stress distribution in the difference problem \mathcal{P}_0 in the form,

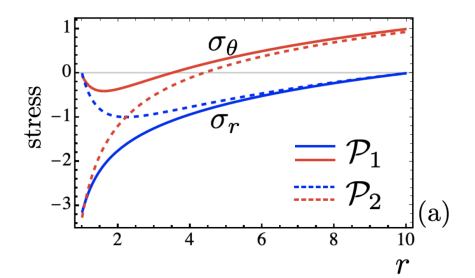
$$\sigma_{r/\theta}^{0} = \frac{R^{2} \sigma_{a}(\pm \psi_{f}^{2} - r^{2})}{r^{2}(1+\nu)(R^{2} - \psi_{f}^{2})} \log \left(\frac{R^{2}(1-\nu) + (1+\nu)\psi_{f}^{2}}{2R^{2}}\right).$$
(168)

If we now compute the associated elastic strain field

$$e_{r/\theta}^{0} = \frac{\sigma_{r/\theta}^{0} - \nu \,\sigma_{\theta/r}^{0}}{E} = c_{1}^{0} \pm \frac{c_{2}^{0}}{r^{2}} \tag{169}$$

where the constants $c_{1/2}^0$ are determined by the boundary conditions. One can see that we obtained the strain distributions of the form (165), which implies that such strains carry no incompatibility. This result is, of course, expected since the addition of the mandrel is equivalent to elastic loading producing purely compatible strains, see Fig.9_b.

We end this section with some comments of physical origin explaining the somewhat counter intuitive presence of compatible residual stresses in the grown coil. Recall that real coils are usually produced using a single continuous tape spiraling onto itself. In contrast, our model coil is produced by adding circular layers. The absence of the continuity of the tape does not produce appreciable



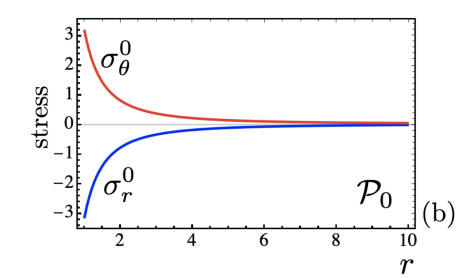


Figure 9: (a-solid) Distribution of radial (σ_r) and hoop (σ_θ) stresses at the end of winding process. These residual stresses are due both to incompatibility and to compatible plastic strains originating from the presence of the rigid core (problem \mathcal{P}_1); (a-dotted) Distribution of radial (σ_r) and hoop (σ_θ) stresses that are due solely to incompatibility (problem \mathcal{P}_2); (b) Distribution of radial (σ_r) and hoop (σ_θ) stresses in the difference problem $\mathcal{P}_0 = \mathcal{P}_1 - \mathcal{P}_2$. Parameters: $\sigma_a = E = 1$, R = 1, D = 1, $\nu = 1/3$.

differences with experimental observations in the winding stage (see e.g. [25]), however, it affects the nature of the subsequent stress relaxation stage.

Thus, if the layers are interconnected, and if the friction is absent, global sliding can fully relax all the stresses. Instead, in our model, which treats layers as independent, only the incompatible contribution to inelastic stresses can be relaxed. Therefore, the contribution to residual stresses due to the compatible part of inelastic strains will survive as we explain in detail in Sec. 6.2.

5.3. Micro-displacement-based approach

We now turn to the description of the same winding protocol using our new general approach, which relies on extended kinematics and is based on the concept of a continuously generated micro-displacement tensor field. As before, we assume that the location of the deposition surface is prescribed in the form $\psi(t) = R + Dt$, which allows us to omit the evolution equation (48). Furthermore, to separate the deposition problem from the relaxation problem (discussed in detail in the the next section), we assume that $\alpha = \infty$ in (46) so that the micro-displacement tensor $\mathbf{U}(\boldsymbol{x})$ is frozen at deposition.

The outer surface is subjected to a prescribed surface micro-scale stress $\sigma_a = \sigma_a e_\theta \otimes e_\theta$, where the winding tension σ_a is a given constant. We also keep the assumptions that winding takes place in 2D and that radial symmetry is maintained. Finally, the macro-displacements are again assumed to be of the form $u(x,t) = u(r,t)e_r$.

5.3.1. Dynamical problem

Given that the normal n to the growth surface coincides with the unit radial vector, $n = e_r$, the natural ansatz for the micro-displacement tensor is of the form

$$\mathbf{U} = \mathbf{V}_{\tau} \star \mathbf{e}_{r}.\tag{170}$$

Furthermore, since the tensor V_{τ} is conjugate to surface stress, these two tensors have the same spectral form and we can write

$$\mathbf{V}_{\tau} = v(r)\mathbf{e}_{\theta} \otimes \mathbf{e}_{\theta} \tag{171}$$

where we took into account that the tensor V_{τ} is assumed to be "frozen" and therefore time-independent. The associated inelastic strain is then

$$\varepsilon_p(r) = -\operatorname{sym}(\operatorname{Curl}(v(r) \star e_r)) = \gamma_r(r)e_r \otimes e_r + \gamma_\theta(r)e_\theta \otimes e_\theta$$
 (172)

where the radial and hoop components are obtained from v(r) as

$$\gamma_r(r) = -\frac{v(r)}{r}, \qquad \gamma_\theta(r) = -v'(r) \tag{173}$$

where we recall that $'=\partial_r$. The dependence of the total strain on macro-displacement must be of a "complementary" form and indeed as we already know

$$\epsilon_r(r,t) = u'(r,t), \qquad \epsilon_\theta(r,t) = \frac{u(r,t)}{r}.$$
(174)

Radial and hoop components of the elastic strain can thus now written in the form

$$e_r(r,t) = u'(r,t) + \frac{v(r)}{r}, \qquad e_\theta(r,t) = v'_r(r) + \frac{u(r,t)}{r}.$$
 (175)

Note that in our previous incremental formulation, the micro-displacement structure of $e_r(r,t)$ and $e_{\theta}(r,t)$ had remained *invisible*.

Radial symmetry also allows to represent the Cauchy stress in the form

$$\boldsymbol{\sigma} = \sigma_r(r, t)\boldsymbol{e}_r \otimes \boldsymbol{e}_r + \sigma_{\vartheta}(r, t)\boldsymbol{e}_{\theta} \otimes \boldsymbol{e}_{\theta} \tag{176}$$

where $(\sigma_r, \sigma_{\vartheta})$ are the radial and hoop components of the stress, constitutively given by the relations

$$\sigma_{r/\theta} = 2\mu \varepsilon_{er/\theta} + \lambda(\varepsilon_{er} + \varepsilon_{e\theta}). \tag{177}$$

With $n = e_r$ and $\mathbf{P}_r = e_\theta \otimes e_\theta$, the surface stress on the growth surface can be written as

$$\overline{\sigma}_{\tau} = \mathbf{P}_{r} \overline{\sigma} \mathbf{P}_{r} = \overline{\sigma}_{\theta} \mathbf{e}_{\theta} \otimes \mathbf{e}_{\theta} \tag{178}$$

where, as before, we adopt the notation $\overline{A}(r) = A(r, \vartheta(r))$ with $\vartheta(r) = (r - R)/D$, to denote the value of a time-dependent field A(r, t) at the instant when the growth surface is located at the radial position r.

At this stage, the unknown fields are u(r,t) and v(r). The equilibrium equation (44) takes the form

$$\sigma_r' + \frac{\sigma_r - \sigma_{\vartheta}}{r} = 0, \qquad R < r < \psi(t). \tag{179}$$

To complete the formulation of the problem we finally add boundary conditions. The "macroscopic" boundary conditions at the deposition surface $r=\psi(t)$ and at the internal core r=R are

$$\begin{cases}
\sigma_r(\psi(t), t) = 0 \\
u(R, t) = 0.
\end{cases}$$
(180)

The corresponding "microscopic" boundary conditions are

$$\begin{cases}
\sigma_{\theta}(\psi(t), t) = \sigma_{a}, \\
v(R) = 0
\end{cases}$$
(181)

After substitution of (177) into $(179)_1$, the latter takes the form

$$w(r,t) - r(w'(r,t) + rw''(r,t)) = 0 (182)$$

where we have introduced, for convenience, the function

$$w(r,t) = u(r,t) + \nu v(r).$$
 (183)

Note that in the incremental macro-scale formulation, the micro-displacement component of w(r,t) had remained invisible.

5.3.2. Solution of the dynamical problem

The general solution of (182) is

$$w(r,t) = A(t)/r + B(t)r. (184)$$

By imposing the boundary conditions (180) we obtain

$$A(t) = \frac{R(1+\nu)\psi(t)\left[R(-1+\nu)\psi(t)\right] - \nu\psi(R)\psi(t)}{R^2(-1+\nu) - (1+\nu)\psi(t)^2}$$
(185)

$$B(t) = \frac{(-1+\nu)\left[R\nu\,v(R) - (1+\nu)\,v(\psi(t))\,\psi(t)\right]}{R^2(-1+\nu) - (1+\nu)\,\psi(t)^2}.$$
 (186)

If we now substitute

$$u(r,t) = A(t)/r + B(t)r - \nu v(r)$$

into $(181)_1$ and use the boundary condition $(181)_2$, we obtain a linear, first order ODE for v(r) whose solution is

$$v(r) = \frac{\sigma_a}{2E} \left(r + \frac{R^2(1-\nu)}{r(1+\nu)} \right) \mathcal{L}(r). \tag{187}$$

Here we have introduced for further convenience an auxiliary function

$$\mathcal{L}(a) = \log\left(\frac{R^2(1-\nu) + a^2(1+\nu)}{2R^2}\right). \tag{188}$$

Using (187) we can also write the explicit expression for macro-displacements

$$u(r,t) = -\frac{\sigma_a}{2rE(1+\nu)} \left[\nu \left(R^2(1-\nu) + r^2(1+\nu) \right) \mathcal{L}(r) + (r^2 - R^2)(1-\nu^2) \mathcal{L}(\psi(t)) \right]. \tag{189}$$

By substituting (189) into (173) we obtain a representation of the inelastic strain in the form

$$\gamma_r(r) = -\frac{\sigma_a}{2E} \frac{R^2(1-\nu) + r^2(1+\nu)}{r^2(1+\nu)} \mathcal{L}(r)$$
(190)

$$\gamma_{\theta}(r) = -\frac{\sigma_a}{2E} \left(2 + \frac{R^2(1-\nu) + r^2(1+\nu)}{r^2(1+\nu)} \mathcal{L}(r) \right). \tag{191}$$

To compare the obtained results with the solution of the macroscopic winding problem we need to compute the expressions for radial and hoop components of the stress $\sigma(x)$, and for the regular and singular components of incompatibility $\eta(x)$. A straightforward substitution shows the full agreements with the results obtained in the previous section by using incremental approach, see our formulas (155),(156),(161),(162). This confirms the equivalence of the two formulations, at least at the level of the macroscopic fields $\sigma(x)$ and $\eta(x)$.

Note, however, that a formal comparison between the expressions of $\boldsymbol{u}(\boldsymbol{x},t)$ and $\varepsilon_p(\boldsymbol{x})$ obtained through the micro-displacement formulation (see Eqs. (189), (190), (191)), and those of $\tilde{\boldsymbol{u}}(\boldsymbol{x},t)$ and $\tilde{\varepsilon}_p(\boldsymbol{x})$ derived within the incremental framework (see Eqs. (154), (159)), reveals a discrepancy. However, the fact that $\boldsymbol{u} \neq \tilde{\boldsymbol{u}}$ and $\varepsilon_p \neq \tilde{\varepsilon}_p$ simply reflects the underlying reparametrization invariance, as ε_p and $\tilde{\varepsilon}_p$ differ by a compatible deformation. Specifically we easily find that

$$\varepsilon_p(\mathbf{x}) - \tilde{\varepsilon}_p(\mathbf{x}) = \operatorname{sym} \nabla \mathbf{g}(\mathbf{x})$$
 (192)

where $g(x) = g(r)e_r$ and

$$g(r) = \frac{R^2(\nu - 1) + r^2(\nu + 1)}{2rE(1 + \nu)} \sigma_a \log \left(\frac{2R^2}{R^2(1 - \nu) + r^2(1 + \nu)} \right).$$
 (193)

As it follows from (189) and (154)

$$q(r) = u(r,t) - \tilde{u}(r,t) \tag{194}$$

which reflects the fact that the compatible component of inelastic strain can be always absorbed into the macro-displacement field and ultimately viewed as a simple re-parametrization of the reference coordinates.

5.3.3. Compatible component of micro-displacement field

As we have shown in Sec.5.2.3, the inelastic strains at the end of the winding process contain, in addition to a component that is responsible for incompatibility, another contribution which is fully compatible and which cannot not be affected by the postulated relaxation mechanism.

Since the micro-displacement tensor serves as the source of the inelastic strain, we can now identify the part of v(r) which is responsible for incompatibility and which can be then viewed as the source of residual stresses in the final configuration after the rigid core is removed.

We begin by identifying the compatible component of the micro-displacement field. Suppose that regular and singular sources of incompatibility are absent and therefore

$$\eta = \gamma_{\theta}'' + \frac{2\gamma_{\theta}' - \gamma_{r}'}{r} = -\frac{v - rv' + 2r^{2}v'' + r^{3}v'''}{r^{3}} = 0$$
 (195)

and

$$\Omega_p = 2\pi R \left(\gamma_{\theta}'(R) + \frac{\gamma_{\theta}'(R) - \gamma_r'(R)}{R} \right) = 2\pi \left(\frac{v(R)}{R} - v'(R) - Rv''(R) \right) = 0.$$
(196

Solving these equations we conclude that a compatible micro-displacement field is of the general form

$$v_c(r) = c_1/r + c_2 r. (197)$$

As expected, the resulting plastic strain components are precisely of the compatible type already discussed in Sec.5.2.3. Specifically, given that

$$\boldsymbol{\beta}_{cp} = (\gamma_{cr}, \gamma_{c\theta}) = -\text{Curl}(\mathbf{V}_{\tau} \star \boldsymbol{e}_r)$$

with

$$\mathbf{V}_{\tau} = v_c \mathbf{P}_{e_r},$$

we obtain that

$$\gamma_{c_r} = -\frac{v_c}{r} = -c_2 - \frac{c_1}{r} \qquad \gamma_{c_\theta} = -v_c' = -c_2 + \frac{c_1}{r}.$$
 (198)

The compatibility means that one can find the corresponding macro-displacement field

$$\boldsymbol{u}(\boldsymbol{x}) = (c_1/r - c_2 r)\boldsymbol{e}_r \tag{199}$$

which has the property $\operatorname{sym} \nabla u \equiv \operatorname{sym}(\operatorname{Curl} \mathbf{U})$ with $\mathbf{U} = \mathbf{V}_{\tau} \star \mathbf{e}_{r}$. In other words, the compatible component of the micro-displacement field $v_{c}(r)$ can be equivalently represented by a macro-displacement field \mathbf{u} .

To find explicitly the compatible field $v_c(r)$ which is relevant for our problem, we need to fix the constants c_1, c_2 by imposing the conditions

$$v_c(R) = v(R), \qquad v_c(\psi_f) = v(\psi_f) \tag{200}$$

where v(r) is the micro-displacement field at the end of winding (187). We obtain

$$c_1 = \frac{R\psi_f(Rv(\psi_f) - \psi_f v(R))}{R^2 - \psi_f^2}, \qquad c_2 = \frac{Rv(R) - \psi_f v(\psi_f)}{R^2 - \psi_f^2}.$$
 (201)

At this point, the incompatible component of the micro-displacement field

$$v_i(r) := v(r) - v_c(r) \tag{202}$$

can be now found explicitly as

$$v_i(r) = \frac{\sigma_a}{2E} (q_1(r) q_2(r) - q_4(r) q_3), \qquad (203)$$

where we have set

$$\begin{cases}
q_{1}(r) = r + \frac{R^{2}(1-\nu)}{r(1+\nu)}, \\
q_{2}(r) = \log\left(\frac{1}{2}\left(1-\nu + \frac{(1+\nu)r^{2}}{R^{2}}\right)\right), \\
q_{3} = \log\left(\frac{1}{2}\left(1-\nu + \frac{(1+\nu)\psi^{2}}{R^{2}}\right)\right), \\
q_{4}(r) = \frac{(r^{2}-R^{2})\left[R^{2}(1-\nu) - (1+\nu)\psi^{2}\right]}{r(1+\nu)(R^{2}-\psi^{2})}.
\end{cases} (204)$$

Note, that in view of (200), the field v_i automatically satisfies the boundary conditions $v_i(R) = v_i(\psi_f) = 0$. Having isolated the incompatible component of the micro-displacement field, we will use the distribution (203) as the initial condition in the relaxation process studied in Sec. 6.2.

5.4. Discussion

In this section we have presented a detailed case study of the process of coil winding under the simplifying assumptions that the rate of material deposition is externally controlled and the attachment-induced micro-displacement field is "frozen", in the sense that there is no post-deposition slip between the deposited layers. The obtained solutions reveal that the micro-displacement tensor field $\mathbf{U}(x)$ necessarily contains compatible and non-compatible additive components. The analysis has shown that the compatible component of $\mathbf{U}(x)$ is due to the rigid constraint provided by the rigid core, and that it relaxes elastically if such core is removed. Instead, the incompatible part of $\mathbf{U}(x)$ persists even after the removal of the mandrel.

In our simplified setting we were able to demonstrate that the macroscopic problem of finding the vector field $\mathbf{u}(\mathbf{x},t)$ can be decoupled from the microscopic problem of finding the micro-displacement tensor field $\mathbf{U}(\mathbf{x})$. We have also shown that the results obtained by solving first the macroscopic problem and then reconstructing the micro-displacement field are perfectly equivalent to the solution of our dynamical problem involving simultaneously the fields $\mathbf{u}(\mathbf{x},t)$ and $\mathbf{U}(\mathbf{x})$.

Although in this particular example both approaches could be used interchangeably, such an equivalence does not hold in general. Thus, in most realistic cases the function $\vartheta(\boldsymbol{x})$ cannot be prescribed a priori and must be computed self-consistently. Similarly, in general the inelastic strains evolve together with

the advancement of the growth surface, therefore these are not "frozen." For instance, as we have already seen in the solidification example discussed in the previous section, the problems for the macro- and micro-displacements could not be decoupled. In such situations, the proposed enriched kinematic framework becomes essential, as an adequate description of the growth process must necessarily involve both $\boldsymbol{u}(\boldsymbol{x},t)$ and $\mathbf{U}(\boldsymbol{x},t)$. The success of such a coupled study is contingent upon the proper treatment of the energetics of deposition.

6. Bulk relaxation of inelastic strain

In the two special cases solved in Sec.4 and Sec.5 we have assumed that no bulk relaxation of the inelastic strain ε_p was allowed after the moment of deposition, meaning that we assumed $\alpha=\infty$ in (46). Here we present a study of a model problem where $\alpha<\infty$ and consider evolution governed by (46). To highlight the relaxational aspect of this example we now assume for simplicity that the deposition process is over and the external boundary remains fixed in its final position at $t=t_f$.

6.1. Relaxation after solidification

Referring to the problem discussed in Sec. 4 while maintaining, in particular, the same horizontal stack geometry, we now assume that at the end of the solidification process the distribution of micro-displacement v(z) is known. The corresponding inelastic strain emerges as an outcome of the deposition stage, and serves as the sole source of residual pre-stress in the grown body which is revealed as soon as the external loads are removed.

We recall that the function v(z) is obtained by integrating Eq. (102) with the condition v(0) = 0 while also using Eq. (110). We obtain

$$v^{0}(z) = \frac{1-\nu}{E} P(p_w - p_a) z \log\left(\frac{z}{\psi_0}\right). \tag{205}$$

The superscript 0 reminds that the corresponding distribution of the microdisplacement is now considered as the initial datum for the relaxation problem. To simplify the analysis of the relaxation stage we neglect the nucleation layer and we consider the unloaded configuration with $s_n = s_w = 0$, defined within the segment (ψ_0, ψ_f) . Note that the dependency of $v^0(z)$ on p_a, p_w is relative to the memory of the loading history, and not to the current loading condition during relaxation.

We assume that during relaxation the system is mechanically equilibrated. This means that in the axial direction we have

$$\sigma_z'(z,t) = 0, \qquad (\psi_0 < z < \psi_f)$$
 (206)

while in the horizontal only the averaged equilibrium condition holds

$$\int_{\psi_0}^{\psi_f} \sigma_{\tau}(z, t) \, dz = 0. \tag{207}$$

Using (206) and the fact that the system is externally unloaded we conclude that $\sigma_z = 0$ and therefore

$$u'(z,t) = \frac{2\nu}{\nu - 1} (\epsilon_{\tau}(t) + v'(z,t)). \tag{208}$$

If we now substitute (208) into the averaged equilibrium equation (207), we obtain

$$\epsilon_{\tau}(t) = -\frac{v(\psi_f, t) - v(\psi_0, t)}{\psi_f - \psi_0}, \qquad \sigma_{\tau}(z, t) = \frac{E}{1 - \nu} (\epsilon_{\tau}(t) + v'(z, t)).$$
(209)

Using the obtained information we can rewrite the evolution equation

$$\sigma_{\tau}'(z,t) = \alpha \dot{v}(z,t) \qquad (\psi_0 < z < \psi_f) \tag{210}$$

in the form

$$\frac{E}{1 - \nu} v''(z, t) = \alpha \dot{v}(z, t) \qquad (\psi_0 < z < \psi_f). \tag{211}$$

It will be convenient to remove from the function v(z,t) an additive part which automatically satisfies (211), which specifically describes compatible micro-displacements.

Indeed, we recall that according to (211) a linear contribution v(z,t) = A(t)z + B(t) would not evolve and, as we have already already seen in Sec.4, would not affect the incompatibility. Therefore we can define the compatible micro-displacement field by the formula $v_c(z) = Az + B$. The time-independent constants A, B can be found by imposing, like we did in (200) for the winding problem, that

$$v_c(\psi_0) = v^0(\psi_0), \qquad v_c(\psi_f) = v^0(\psi_f)$$
 (212)

where $v^0(z)$ is given by (205). We thus obtain

$$v_c(z) = \frac{P(p_w - p_a)(1 - \nu)(z - \psi_0)\psi_f}{E(\psi_0 - \psi_f)} \log\left(\frac{\psi_f}{\psi_0}\right).$$
 (213)

The incompatible component of the micro-displacement, which relaxes according to (211), may can be computed as

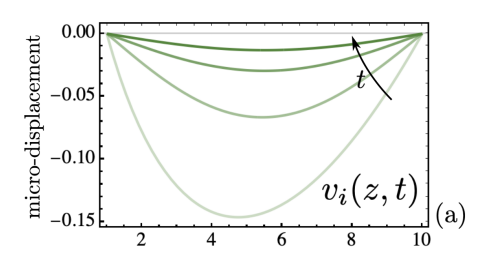
$$v_i(z,t) = v(z,t) - v_c(z)$$
 (214)

where by definition $v_i(\psi_0, t) = v_i(\psi_f, t) = 0$, and where the initial value is

$$v_i^0(z) = v^0(z) - v_c(z). (215)$$

The ensuing evolution problem for $v_i(z,t)$ takes the form

$$\begin{cases} v_i''(z,t) = \omega^2 \dot{v}(z,t) & (\psi_0 < z < \psi_f) \\ v_i(z,0) = v_i^0(z) & \\ v_i(\psi_0,t) = v_i(\psi_f,t) = 0 \end{cases}$$
 (216)



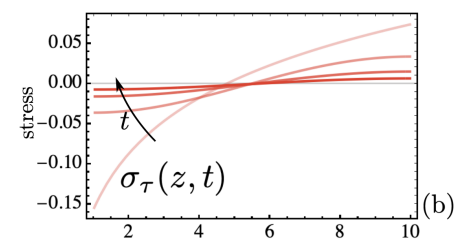


Figure 10: Evolution of the horizontal stress (a) and incompatible micro-displacement (b) during the stress relaxation stage. Darker colors indicate more recent time instants. Parameters: $\sigma_a = E = 1, R = 1, D = 1, \nu = 1/3, \lambda = 10$.

where we introduced the notation $\omega^2 = \alpha(1 - \nu)/E$. The problem (216) is formulated for a linear diffusion equation which can be solved explicitly, with results illustrated in Fig. 10.

According to Fig. 10, as time increases, the magnitude of incompatible micro-displacement $v_i(z,t) = v(z,t) = v_c(z)$ decreases throughout the whole domain. This fully relaxes residual elastic stresses at the end of the process.

The only component of the micro-displacement that survives at the end of the relaxation process is the one describing compatible deformation and defined by (213). According to (209)₁, where we set $v(r, \infty) = v_c(r)$, this component is responsible for a residual lateral strain

$$\epsilon_{\tau} = \frac{P(p_w - p_a)(1 - \nu)\psi_f}{E(\psi_0 - \psi_f)} \log\left(\frac{\psi_f}{\psi_0}\right). \tag{217}$$

Similarly from $(209)_2$ we infer that at $t = \infty$ the lateral stress σ_{τ} will fully relax.

6.2. Relaxation after winding

Consider next our second example where the pre-stressed configuration was obtained through winding a coil. We now assume that winding is complete and that the external boundary remains fixed in its final position at $t = t_f$, and starting from this final state we allow the incompatibility to relax according to (46). One of our goals will be to show that, once again, only the incompatible part of the micro-displacement field is involved in such relaxation process.

Specifically, we assume that a grown coil of radius ψ_f carries the initial micro-displacement distribution of the form

$$v(r,0) = v_0(r) \equiv \frac{\sigma_a}{2E} \left(r + \frac{R^2(1-\nu)}{r(1+\nu)} \right) \log \left(\frac{R^2(1-\nu) + r^2(1+\nu)}{2R^2} \right).$$
 (218)

Under the assumption of radial symmetry the governing equations (44)–(46) can be presented in the form of a system:

$$R < r < \psi_f: \begin{cases} \sigma_r' + \frac{\sigma_r - \sigma_{\vartheta}}{r} = 0\\ \sigma_{\theta}' + \frac{\sigma_{\theta} - \sigma_r}{r} = \alpha \dot{v} \end{cases}$$
 (219)

During relaxation, once again we find that the equilibrium equation $(219)_1$ is satisfied as long as

$$u(r,t) = A(t)/r + B(t)r - \nu v(r,t)$$
(220)

where differently than in (183), the function v(r,t) now depends also on time. The functions A(t), B(t) are obtained by imposing the boundary conditions

$$\begin{cases} \sigma_r(\psi_f, t) = 0\\ u(R, t) = 0. \end{cases}$$
 (221)

For the coefficients A(t), B(t) we naturally recover the same expressions (185), (186) as in the previous section.

Upon substitution of the obtain relations into $(219)_2$, we end up with a linear PDE with variable coefficients, describing the relaxation of the micro-displacement field

$$\alpha \dot{v}(r,t) = -\frac{E}{r} \left(\frac{v(r,t)}{r} - v'(r,t) - rv''(r,t) \right). \tag{222}$$

Once again, if the micro-displacement field is compatible, $v(r,t) \equiv v_c(r,t)$ where, from (197),

$$v_c(r,t) = c_1/r + c_2 r (223)$$

with $c_{1/2}(t)$ arbitrary functions of time, then equation (222) reduces to

$$\dot{v}_c(r,t) = 0 \tag{224}$$

suggesting that for $v_c(r,t)$ to be a solution of (222), the coefficients $c_{1/2}$ not depend on time, and therefore such micro-displacement field should be "frozen",

$$v_c(r,t) = v_c(r). (225)$$

Because the compatible component of the micro-displacement field v(r,t) cannot change, only its incompatible component defined in (202) will be evolving during the relaxation process described by (219)₂. In other words, the relaxation of the incompatible part of inelastic strain can be decoupled from the "frozen" compatible part. The latter can be, of course, relaxed elastically by removing the mandrel without engaging a dissipative process.

To summarize, similar to what we have seen in the case of post solidification relaxation, here again the relaxation process described by (46) only concerns the function

$$v_i(r,t) := v(r,t) - v_c(r)$$
 (226)

where the compatible component $v_c(r)$ was determined in Sec.5.3.3. The corresponding initial conditions are known since we have the expression for $v_0(r)$ from (218) and can write

$$v_i(r,0) := v_0(r) - v_c(r). (227)$$

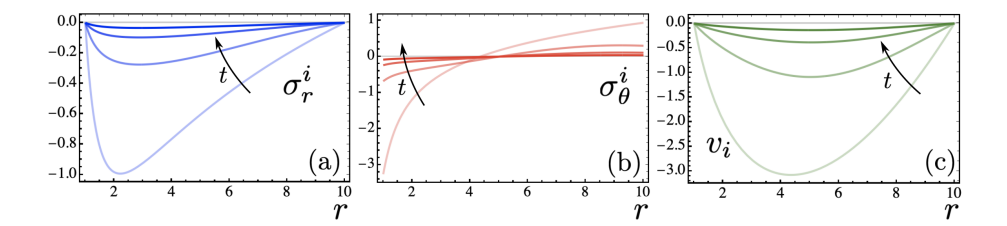


Figure 11: Evolution of the radial (a) and hoop (b) stress components, along with microdisplacement (c) during the stress relaxation stage. Darker colors indicate more recent time instants. Parameters: $\sigma_a = E = 1$, R = 1, D = 1, $\nu = 1/3$, $\lambda = 10$.

Since by definition

$$v_i(R,0) = v_i(\psi_f, 0) = 0 (228)$$

we assume that the same boundary conditions hold throughout the whole relaxation process, so that

$$v_i(R,t) = v_i(\psi_f, t) = 0.$$
 (229)

As we now focus on the evolution of $v_i(r,t)$ with boundary conditions $v_i(R,t) = v_i(\psi_f,t) = 0$, we set A = B = 0. The associated macro-displacements can be found from $u(r,t) = -\nu v_i(r,t)$.

The equations governing the evolution of the incompatible micro-displacement field take the form

$$\begin{cases} \alpha \dot{v}_i(r,t) = -E\left(v_i(r,t)/r - v_i'(r,t) - rv_i''(r,t)\right)/r \\ v_i(r,0) = v_i^0(r) \\ v_i(R,t) = 0 \\ v_i(\psi_f,t) = 0. \end{cases}$$
(230)

The problem $(230)_1$ involves a linear parabolic partial differential equation, of basically the same type as the equation obtained in the study of relaxation of solidification stresses, see (216). The right-hand side of $(230)_1$ involves the radial part of the Laplacian acting on the incompatible micro-displacement field $v_i(r,t)$, while the left-hand side introduces a viscous/relaxation time scale proportional to α . From the solution to (230) we can find the incompatible elastic strains

$$\epsilon_r^i = u' + v_i/r, \qquad \epsilon_\theta^i = v_i' + u/r$$
 (231)

and we can compute the associated components of stress, as exclusively induced by incompatibility

$$\sigma_r^i(r,t) = Ev_i(r,t)/r, \qquad \sigma_\theta^i(r,t) = Ev_i'(r,t). \tag{232}$$

The numerical solution to the problem (230) is illustrated in Fig. 11. As expected, the incompatibility-related part of stress and the associated micro-displacement both relax to zero. By the end of relaxation, the coil remains residually stressed due to the non-relaxing contribution $\sigma_{r/\theta}^0(r)$ from (168) which, as we have seen, can be eliminated only through the removal of the rigid core.

We emphasize once again that the persistence of residual stress after relaxation stems from the way the winding problem was formulated. In particular, by neglected the continuity of the tape and treating the winding process as sequential deposition of independent layers, we have eliminated the possibility for global "unwinding" relaxation modes. While the simplifications introduced here are justified by the resulting analytical transparency, further investigations are required for cases in which interlayer friction is overcome, thereby allowing the ensuing global relaxation process to completely eliminate the residual stresses within the coil [91].

6.3. Discussion

In this section we have presented two simple models of bulk relaxation of inelastic strains accumulate during the process of surface deposition. We have assumed that relaxation is of a purely viscous (Onsagerian) type, while it could also be of a threshold type, as in dry friction and crystal plasticity. In this sense the adopted model can be viewed as representing a form of linear viscoelasticity.

Our analysis reveals a fundamental decoupling between the compatible and incompatible components of the micro-displacement field: only the incompatible part evolves in time, while the compatible component remains "frozen" in its initial state. This indicates that the relaxation process in the adopted model is governed solely by incompatibility, which undergoes a dissipative evolution until the micro-displacement tensor becomes fully compatible. The resulting configuration thus preserves the residual stresses associated with the displacement-controlled boundary, as these cannot relax through the considered dissipative mechanism.

7. Conclusions

The goal of this paper is to develop an extended kinematics of continuum elastic bodies allowing one to address micro-mechanical interactions involved in the accumulation and storage of mechanical "information" inside a solid body. The main assumption is that such "information" is carried by geometrical *incompatibility*, which can be revealed, for instance, by cutting the unstressed body into smaller sub-bodies while recording the resulting deformation.

We are therefore concerned with the question of how the incompatibility can be *inserted* into a solid body, and how the acquired mechanical "information" may be *erased* by internal dissipative relaxation.

The growing attention to such issues is mainly due to the emergence of novel applications of solid mechanics in the fields of biomechanics and bio-mimetic technology, where the task of microscopically supervised storage and maintenance of the incompatibility has recently come to the forefront, see [6, 8, 9, 10, 67, 68] and the literature cited therein. It was found, for instance, that biological systems can develop incompatibility by using metabolically supported mechanical pathways, ultimately representing microscopic mechanical activity [92]. Viewing incompatibility as being managed through internal activity, we

have focused in this work on a specific case of controlled surface growth in non-Euclidean solids, where the role of the active microscopic mechanical "agents" responsible for inserting mechanical "information" can, for instance, be played by a 3D printer [7].

To shed light on the basic interplay between macro- and micro- mechanics in the process of active manipulation of incompatibility, we developed in this paper a novel kinematic approach in the general framework of continuum mechanics which explicitly identifies microscopic variables that are potentially acted upon by such microscopic active "agents".

Our approach is built around the concept of micro-displacement tensor, which complements the conventional kinematic description of solids based on the idea of a macro-displacement vector. Given that the physical dimensionality of macro-displacement vector and micro-displacement tensor is the same, in both cases the corresponding conjugate variables can be identified as forces. However, if in the conventional macroscopic theory such forces are represented by vectors, their microscopic counterparts emerge as couples, represented by tensors. We have shown that the proposed approach allows one to model the externally imposed micro-mechanical controls at the boundary of the growing body which go beyond the conventional three components of surface tractions. Instead, rather counter-intuitively, they are adequately represented by prescribing on the boundary of all six components of the macroscopic stress tensor.

The idea that in a growing body, active micro stresses can effectively control the emerging incompatibility was (even if implicitly) present in several previous studies [15, 18, 25, 19, 14, 17]. However, while some of these earlier treatments have already imposed a phenomenological assumption that the total state of stress is prescribed on the growth surface, they did not operate with the concept of micro-displacements and therefore could not adequately account for the energetic cost of the implied microscopic activity. Also, in most of these works, the motion of the deposition surface was not treated self-consistently, as it was either prescribed from outside, or it was attributed to a largely decoupled physical process, such as the removal of the released heat. Instead, we showed that micro-forces may play a significant role in mechanically regulated kinetics of deposition, by even deciding the outcome of its long term evolution.

As there are still many challenges on the way of rigorous up-scaling of the newly defined microscopic quantities directly from the microscale, our approach to the *energetics* of surface deposition is purely phenomenological. Specifically, we have developed our extended continuum mechanical description of associated active micro-mechanical processes with the reference to a simple layering *ansatz* for the micro-displacement tensor, and by using only the most basic symmetry considerations and thermodynamic inequalities.

Using only classical thermodynamic considerations, we succeeded in deriving the equations governing both the process of incompatibility acquisition at the surface of the growing body, and the subsequent evolution of incompatibility past the initial state of deposition. In physical terms, our main assumption was that incompatibility can be generated by generalized micro-forces operating during deposition on the growth surface, and that its quasi-viscous relaxation

can be in principle controlled by the action of the generalized micro-forces, operating inside the growing body. While the former are exemplified by the agency responsible for the pre-stretch of the attached elastic bands, the latter can be pictured, for instance, as frictional forces preventing slips between adjacent deposition layers.

We have illustrated our general constructions by three detailed case studies. The goal was to show how the proposed *general* approach works in detail in *special* situations, where geometrical and physical simplicity of the setting makes the problem amenable to an analytically transparent treatment.

Our first example addresses the classical solidification phenomenon, where we assumed that the deposited solid material can be internally pre-stressed in the process of liquid-to-solid transition. While most previous studies of solidification had framed the problem within the "elastic growth" setting, with solid phase growing incompatibility-free [49, 48, 66], the introduction of a richer kinematics has allowed us to extend the description to the case of "inelastic growth", where the account of the work of microscopically generated active surface stresses underlines their crucial role in the acquisition of incompatibility.

Our second example can be interpreted as a minimal model of a winding process around a rigid mandrel, developed under the simplifying assumptions that the rate of material deposition is externally controlled and that the attachment-induced inelastic strain is "frozen" immediately after deposition. In this setting, we demonstrated that the macroscopic problem of determining the classical displacement field and the microscopic problem of determining the incompatibility tensor can be decoupled. We further showed that the pre-stretch of the deposited layers may give rise not only to incompatibility but also to compatible inelastic strain.

Our final example addressed the bulk relaxation of preexisting incompatibility, showing that only part of the growth-induced pre-stress can relax through the proposed viscous mechanism. Specifically, the analysis revealed a fundamental decoupling between the compatible and incompatible components of the micro-displacement field: only the incompatible part evolves under the adopted mechanism, while the compatible component remains "frozen" in its initial state.

It is important to mention that while in our three case studies we considered *separately* such aspects of the surface deposition problem as the possibility of mechanically regulated self-consistent growth, the unavoidable emergence of compatible inelastic strain and the peculiarity of mechanically controlled bulk relaxation of inelastic strain, in general applications one can expect that all these effects will appear *together* and that only their delicate interplay will ultimately decide the mechanical outcome of the surface deposition process.

The proposed model can be extended and enriched along several directions. An important first step could be the development of a finite strain version of the same approach, e.g. [10]. A microscopically informed derivation of such nonlinear model should allow one to establish a formal link of the proposed approach with the theory of second-order structured deformations, e.g. [93]. However, the corresponding extended theory should not be restricted by the layering ansatz and should also account for the possibility of non-layering arrangement of the

deposited material. For instance, while considerable simplification was achieved in this paper due to the simplifying assumption that the field prescribing the orientation of the layering in the bulk is effectively "frozen" and does not evolve past deposition, such an assumption is clearly not sufficiently general. Similarly, our assumption regarding the Onsagerian nature of relaxation can be questioned, for instance, one may argue that micro-displacements should relax in non-Onsagerian way as, for instance, in dry friction and plasticity. Furthermore, a more intricate coupling between micro and macro displacements can be imagined, for instance, in various biological applications one can expect that it is not even reciprocal [94].

An important step towards applications could be an adaptation of the proposed theory to particular technologically relevant modalities of 3D printing, including a specification of the mechanical micro-activity defining the writing head, e.g. [7]. Another challenge is the adaptation of the developed general theory to specific problems involving the manipulation of incompatibility in living systems, where the abstract active "agents" would have to be identified with the specific molecular micro-machines exposed to metabolic energy sources, e.g [95].

8. Acknowledgments

The authors thank B. Shoykhet and P. Recho for helpful discussions. L.T. acknowledges the support under the grants ANR-17-CE08-0047-02, ANR-21-CE08-MESOCRYSP an 2020-MSCA-RISE-2020-101008140. G.Z. gratefully acknowledges the kind hospitality extended by Politecnico di Bari while hosting his sabbatical leave from January to June 2025, where part of this research was conducted.

References

- [1] Y. Han, Y. Shokef, A. Alsayed, et al., Geometric frustration in buckled colloidal monolayers, Nature 456 (2008) 898–903.
- [2] M. Moshe, M. J. Bowick, and marchetti, M. Cristina, Geometric Frustration and Solid-Solid Transitions in Model 120 (2018) 268105.
- [3] A. Gabrielov, V. Keilis-Borok, D. D. Jackson, Geometric incompatibility in a fault system, Proc. Natl. Acad. Sci. USA 93 (1996) 3838–3842.
- [4] A. Ziepke, I. Maryshev, I. S. Aranson, et al., Multi-scale organization in communicating active matter, Nat Commun 13 (2022) 6727.
- [5] R. D. Baker, T. Montenegro-Johnson, A. D. Sediako, M. J. Thomson, A. Sen, E. Lauga, I. S. Aranson, Shape-programmed 3d printed swimming microtori for the transport of passive and active agents, Nat Commun 10 (1) (2019) 4932.
- [6] D. Renzi, S. Marfia, G. Tomassetti, G. Zurlo, A discrete model for layered growth, europ, Journal of Mechanics A/Solids 105 (105232) (2024) 13.

- [7] D. Zaza, M. Ciavarella, G. Zurlo, Strain incompatibility as a source of residual stress in welding and additive manufacturing, europ, J. Mechanics A/Solids 85 (2021) 104147.
- [8] G. Zurlo, L. Truskinovsky, Printing non-euclidean solids, Physical Review Letters 119 (2017) 048001.
- [9] G. Zurlo, L. Truskinovsky, Inelastic surface growth, Mechanics Research Communications 93 (2018) 174–179.
- [10] L. Truskinovsky, G. Zurlo, Nonlinear elasticity of surface growth, Phys. Rev. E 99 (2019) 053001.
- [11] C. Eckart, The thermodynamics of irreversible processes, IV. The Theory of Elasticity and Anelasticity, Physical Review 73 (4) (1948) 373–382.
- [12] Y. Wang, S. E. Naleway, B. Wang, Biological and bioinspired materials: Structure leading to functional and mechanical performance, Bioactive Materials 5 (4) (2020).
- [13] G. Volpe, C. Bechinger, F. Cichos, et al., Active matter in space, npj Microgravity 8 (2022) 54.
- [14] R. V. Southwell, An Introduction to the Theory of Elasticity for Engineers and Physicists, Oxford university press; 2d ed edition, 1941.
- [15] V. K. Trincher, Formulation of the problem of determining the stress-strain state of a growing body, Izv. AN SSSR. Mekhanika Tverdogo Tela 19 (2) (1984) 119–124.
- [16] V. A. Pal'mov, On stresses originating during material solidification, Inzh. Zh. Mekh. Tverd. Tela 4 (1967) 80–85.
- [17] C. B. Brown, L. E. Goodman, Gravitational stresses in accreted bodies, Proc. R. Soc. London, Ser. A, Math. Phys. Sci. 276 (1367) (1963) 571–576.
- [18] W. D. King, N. H. Fletcher, Pressures and stresses in freezing water drops, J. Phys. D 6 (18) (1973) 21–57.
- [19] E. I. Rashba, Determining stresses in massive structures originating from their own weight: The effect of the construction sequence, in: Proc. Inst. Civil Engin. of Acad. Sci. of Ukrain. SSR 18, 1953, pp. 23–27.
- [20] N. K. Arutyunyan, Boundary value problem of the theory of creep for a body with accretion, J. Appl. Math. and Mech. 41 (5) (1977) 804–810.
- [21] V. V. Metlov, On the accretion of inhomogeneous viscoelastic bodies under finite deformations p. m. m, USSR 49 (4) (1985) 490–498.
- [22] V. E. Naumov, Indentation of a growing die into a viscoelastic rod-type foundation, Mech. of Solids 23 (3) (1988) 80–89.

- [23] V. E. Naumov, Mechanics of growing deformable solids: a review, J. Eng. Mech. 120 (1994) 207–220.
- [24] A. N. Kh, A. V. Manzhirov, Contact problems of the mechanics of bodies with accretion, P. M. M. U. S. S. R. 53(l) (1989) 117–128.
- [25] N. Zabaras, S. Liu, A theory for small deformation analysis of growing bodies with an application to the winding of magnetic tape packs, Acta mechanica 111 (1) (1995) 95–110.
- [26] R. Skalak, A. Hoger, Kinematics of surface growth, J. Math. Biol. 35 (1997) 869.
- [27] A. Drozdov, Continuous accretion of a composite cylinder, Acta mechanica 128 (1) (1998) 117–135.
- [28] A. Bacigalupo, L. Gambarotta, Effects of layered accretion on the mechanics of masonry structures, Mech. Based Design Struct. Mach. 40 (2012) 163.
- [29] P. Ciarletta, L. Preziosi, G. Maugin, Mechanobiology of interfacial growth, Journal of the Mechanics and Physics of Solids 61 (3) (2013) 852–872.
- [30] G. Tomassetti, T. Cohen, R. Abeyaratne, Steady accretion of an elastic body on a hard spherical surface and the notion of a four-dimensional reference space, Journal of the Mechanics and Physics of Solids 96 (2016) 333–352.
- [31] D. Swain, A. Gupta, Biological growth in bodies with incoherent interfaces, Proc. R. Soc. A 474, article 20170716 (2018).
- [32] R. Abi-Akl, R. Abeyaratne, T. Cohen, Kinetics of surface growth with coupled diffusion and the emergence of a universal growth path, Proc. R. Soc. A 475, article 20180465 (2019).
- [33] S. K. Naghibzadeh, N. Walkington, K. Dayal, Surface growth in deformable solids using an eulerian formulation, Journal of the Mechanics and Physics of Solids 154 (2021) 104499.
- [34] S. P. Pradhan, A. Yavari, Accretion—ablation mechanics, Philosophical Transactions of the Royal Society A: Mathematical, Physical and Engineering Sciences 381 (2263) (2023) 20220373, 10.1098/rsta.2022.0373.
- [35] A. Yavari, Y. Safa, A. Soleiman Fallah, Finite extension of accreting nonlinear elastic solid circular cylinders, Continuum Mechanics and Thermodynamics 36 (5) (2024) 1053–1069.
- [36] G. Cicconofri, P. Blanco, G. Vilanova, P. Sáez, M. Arroyo, Active interfacial degradation/deposition of an elastic matrix by a fluid inclusion: Theory and pattern formation, Journal of the Mechanics and Physics of Solids 191 (2024) 105773.

- [37] D. Riccobelli, Elastocapillarity-driven surface growth in tumour spheroids, arXiv preprint (2024). arXiv:2410.03344.
- [38] E. Beltrami, Osservazioni sulla nota precedente, Att. Accad. Nazl. Lincei 1 (1892) 141–142.
- [39] R. Fosdick, G. Royer Carfagni, A stokes theorem for second-order tensor fields and its implications in continuum mechanics, International Journal of Non-Linear Mechanics 40 (3) (2005) 381–386.
- [40] M. Gurtin, E, in: Linear Theories of Elasticity and Thermoelasticity, -, Springer, New York, 1973, pp. 1–295.
- [41] G. B. Maggiani, R. Scala, N. Van Goethem, A compatible-incompatible decomposition of symmetric tensors in lp with application to elasticity math, Meth. Appl. Sci. 38 (2014) 5217–5230.
- [42] D. Owen, R. Paroni, Second-order structured deformations, Arch. Rational Mech. Anal. 155 (2000) 215–235.
- [43] R. Paroni, Second-order structured deformations: Approximation theorems and energetics, in: G. Del Piero, D. R. Owen (Eds.), Multiscale Modeling in Continuum Mechanics and Structured Deformations. International Centre for Mechanical Sciences, vol 447., Vienna, Springer, 2004, pp. 177–202.
- [44] J. Nye, Some geometrical relations in dislocated crystals, Acta Metallurgica 1 (1953) 152–162. doi:10.1016/0001-6160(53)90054-6.
- [45] J. D. Jackson, Classical Electrodynamics, 3rd Edition, John Wiley & Sons, New York, 1998.
- [46] M. E. Gurtin, Introduction to Continuum Mechanics, London/, Academic Press, New York, 1981.
- [47] J. W. Gibbs, On the equilibrium of heterogeneous substances, Arts Sci. 524 (1878) 108–248, translated by Connecticut Acad Article 1877-1878. 3, (1775-1876), 343.
- [48] R. F. Sekerka, J. W. Cahn, Solid-liquid equilibrium for non-hydrostatic stress, Acta Materialia 52 (6) (2004) 1663–1668.
- [49] B. E. Hobbs, A. Ord, Does non-hydrostatic stress influence the equilibrium of metamorphic reactions?, Earth-Science Reviews 163 (2016) 190–233.
- [50] I. M. Kaganova, A. L. Roitburd, Equilibrium between elastically-interacting phases, Sov. Phys. JETP 67 (6) (1988).
- [51] I. M. Lifshits, L. S. Gulida, On nucleation under local melting, Dokl. Akad. Nauk SSSR 87 (4) (1952) 523–526, (In Russian; English version available.).

- [52] V. I. Levitas, Thermomechanical theory of martensitic phase transformations in inelastic materials, International Journal of Solids and Structures 35 (8) (1998) 889–940.
- [53] S. J. S. Morris, Interface kinetics, grain-scale deformation, and polymorphism, Annual Review of Earth and Planetary Sciences 45 (1) (2017) 245–269.
- [54] L. Truskinovsky, The equilibrium of a spherical nucleus with the matrix in solid state transformation, Geochemistry International 3 (1984) 443–447.
- [55] L. Truskinovsky, The chemical potential tensor, Geochemistry International 12 (1983) 1730–1744.
- [56] T. Frolov, Y. Mishin, Effect of nonhydrostatic stresses on solid-fluid equilibrium. i. bulk thermodynamics, Physical Review B—Condensed Matter and Materials Physics 82 (17) (2010) 174113.
- [57] H. W. Green, On the thermodynamics of non-hydrostatically stressed solids, Philosophical Magazine A 41 (5) (1980) 637–647.
- [58] J. Ghoussoub, Y. M. Leroy, Solid–fluid phase transformation within grain boundaries during compaction by pressure solution, Journal of the Mechanics and Physics of Solids 49 (10) (2001) 2385–2430.
- [59] R. M. Bowley, Instabilities of the liquid-solid interface, Journal of Low Temperature Physics 89 (1) (1992) 401–415.
- [60] R. Myhill, Chemical potentials in non-hydrostatically stressed anisotropic phases, Geophysical Journal International 241 (2) (2025) 1042–1052.
- $[61]\;$ J. F. Nye, Theory of regelation, The Philosophical Magazine 16 (144) (1967) 1249–1266.
- [62] M. Angelillo, A. Fortunato, A. Montanino, M. Lippiello, Singular stress fields in masonry structures, Derand was right, Meccanica 49 (2014) 1243– 1262.
- [63] M. Silhavy, Cauchy's stress theorem for stresses represented by measures, Continuum Mechanics and Thermodynamics 20 (2008) 75–96.
- [64] P. Podio-Guidugli, Examples of concentrated contact interactions in simple bodies, Journal of Elasticity 75 (2005) 167–186.
- [65] A. Pandey, A. Gupta, Point singularities in incompatible elasticity, Journal of Elasticity 147 (1) (2021) 229–256.
- [66] Y. Grabovsky, L. Truskinovsky, A class of nonlinear elasticity problems with no local but many global minimizers, J Elast 154 (2023) 147–171.

- [67] A. Erlich, G. Zurlo, Incompatibility-driven growth and size control during development j, Mech. Phys. Solids 188 (2024) 105660.
- [68] A. Erlich, G. Zurlo, The geometric nature of homeostatic stress in biological growth, Journal of the Mechanics and Physics of Solids 201 (2025) 106155.
- [69] J. G. Dash, J. S. Rempel A. W. Wettlaufer, The physics of premelted ice and its geophysical consequences, Reviews of Modern Physics 78 (2006) 695.
- [70] F. Montel, M. Delarue, J. Elgeti, L. Malaquin, M. Basan, T. Risler, B. Cabane, D. Vignjevic, J. Prost, G. Cappello, J.-F. Joanny, Stress clamp experiments on multicellular tumor spheroids, Phys. Rev. Lett. 107 (18) (2011) 188102.
- [71] L. A. Taber, Towards a unified theory for morphomechanics, Phil. Trans. R. Soc. A 367 (2009) 3555–3583.
- [72] B. I. Shraiman, Mechanical feedback as a possible regulator of tissue growth, PNAS 102 (9) (2005) 3318–3323.
- [73] R. J. Asaro, W. A. Tiller, Interface morphology development during stress corrosion cracking: Part i. via surface diffusion, Metall. Trans. 3 (1972) 1789–1796.
- [74] M. A. Grinfeld, Instability of the equilibrium of a nonhydrostatically stressed body in the presence of surface melting, Sov. Phys. Dokl. 31 (1986) 831–834.
- [75] Y. Grabovsky, L. Truskinovsky, Roughening instability of broken extremals, Arch Rational Mech Anal 200 (2011) 183–202.
- [76] J. F. Lutsko, G. Nicolis, Theoretical evidence for a dense fluid precursor to crystallization, Physical Review Letters 96 (4) (2006) 046102.
- [77] J. W. Mullin, Crystallization, 4th Edition, Elsevier, 2001.
- [78] V. I. Yukalov, Theory of melting and crystallization, Physical Review B 32 (1) (1985) 436–446.
- [79] I. M. Svishchev, P. G. Kusalik, Crystallization of liquid water in a molecular dynamics simulation, Physical Review Letters 73 (7) (1994) 975–978.
- [80] S. T. Yau, B. R. Thomas, P. G. Vekilov, Molecular mechanisms of crystallization and defect formation, Physical Review Letters 85 (2) (2000) 353–356.
- [81] N. Perez, Solidification heat transfer, in: N. Switzerland (Ed.), Materials Science, Springer, Cham, 2024, pp. 379–457.

- [82] D. M. Stefanescu, R. Ruxanda, Fundamentals of solidification, ASM Handbook 9, metallography and Microstructures, ASM International (2004).
- [83] B. Chalmers, Principles of solidification, in: E. A. Brandes (Ed.), Applied Solid State Physics, Boston, MA, Springer US, 1964, pp. 161–170.
- [84] H. Hu, S. A. Argyropoulos, Mathematical modelling of solidification and melting: a review, Modelling and Simulation in Materials Science and Engineering 4 (4) (1996) 371–396.
- [85] W. Kurz, D. Fisher, M. Rappaz, Fundamentals of Solidification, Net, Scientific, 2023.
- [86] J. K. Good, D. R. Roisum, Winding: machines, mechanics and measurements, DEStech Publications, INC, 2008.
- [87] K. Ärölä, R. V. Hertzen, Two-dimensional axisymmetric winding model for finite deformation, Computational Mechanics 40 (2007) 933–947.
- [88] K. T. Park, H. C. Park, Effects of design parameters and tension on behavior of a coil using finite element analysis, Journal of Iron and Steel Research International 25 (2018) 883–891.
- [89] F. R. de Hoog, M. Cozijnsen, W. Y. D. Yuen, An inverse solution for winding stresses in wound coils of linear orthotropic material with large deformations, Proceedings of the Institution of Mechanical Engineers, Part C: Journal of Mechanical Engineering Science 221 (6) (2007) 639–652.
- [90] P. Krysiak, A. Błachut, J. Kaleta, Theoretical and experimental analysis of inter-layer stresses in filament-wound cylindrical composite structures, Materials 14 (22) (2021) 7037.
- [91] M. Caelen, S. Moulinet, B. Andreotti, F. Lechenault, Tightening dynamics of wound rolls: The interplay of solid friction and interfacial compressibility, hal-03659906v2 (2025).
- [92] R. Farhadifar, J.-C. Röper, B. Aigouy, S. Eaton, F. Jülicher, The influence of cell mechanics, cell-cell interactions, and proliferation on epithelial packing, Current Biology 17 (24) (2007) 2095–2104.
- [93] J. Matias, M. Morandotti, D. R. Owen, Energetic relaxation to structured deformations: A multiscale geometrical basis for variational problems in continuum mechanics, Springer Singapore (2023).
- [94] G. G. Lorenzana, D. Martin, Y. Avni, D. S. Seara, M. Fruchart, G. Biroli, V. Vitelli, When is nonreciprocity relevant?, arXiv preprint arXiv:2509.17972 (2025).
- [95] F. Jülicher, S. W. Grill, G. Salbreux, Hydrodynamic theory of active matter, Reports on Progress in Physics 81 (7) (2017) 076601.